A&A 665, A95 (2022)
https://doi.org/10.1051/0004-6361/202243931

Astronomy & Astrophysics

The miniJPAS survey: A search for extreme emission-line galaxies

J. Iglesias-Páramo[1], A. Arroyo[1], C. Kehrig[1], J. M. Vílchez[1], S. Duarte Puertas[16,1], E. Pérez-Montero[1], I. Breda[1], Y. Jiménez-Teja[1], C. López Sanjuan[15], A. Lumbreras-Calle[2], P. Coelho[3], S. Gurung-López[4,5], C. Queiroz[13], I. Márquez[1], M. Pović[17,1], R. González Delgado[1], J. Chaves-Montero[7], D. Sobral[11,12], A. Hernán-Caballero[2], J. A. Fernández-Ontiveros[2], L. A. Díaz-García[1], A. Alvarez-Candal[1,14,6], R. Abramo[3], J. Alcaniz[6], N. Benítez[1], S. Bonoli[7,8,2], A. J. Cenarro[15], D. Cristóbal-Hornillos[2], R. Dupke[6], A. Ederoclite[2], A. Marín-Franch[15], C. Mendes de Oliveira[9], M. Moles[2], L. Sodré Jr.[9], K. Taylor[10], J. Varela[15], H. Vázquez-Ramió[15], and J-PAS team

(*Affiliations can be found after the references*)

Received 3 May 2022 / Accepted 22 June 2022

ABSTRACT

Context. Galaxies with extreme emission lines (EELGs) may play a key role in the evolution of the Universe, as well as in our understanding of the star formation process itself. For this reason an accurate determination of their spatial density and fundamental properties in different epochs of the Universe will constitute a unique perspective towards a comprehensive picture of the interplay between star formation and mass assembly in galaxies. In addition to this, EELGs are also interesting in order to explain the reionization of the Universe, since their interstellar medium (ISM) could be leaking ionizing photons, and thus they could be low z, analogous of extreme galaxies at high z.

Aims. This paper presents a method to obtain a census of EELGs over a large area of the sky by detecting galaxies with rest-frame equivalent widths ≥300 Å in the emission lines [OII]$\lambda\lambda$3727,3729Å, [OIII]λ5007Å, and Hα. For this, we aim to use the J-PAS survey, which will image an area of ≈8000 deg^2 with 56 narrow band filters in the optical. As a pilot study, we present a methodology designed to select EELGs on the miniJPAS images, which use the same filter dataset as J-PAS, and thus will be exportable to this larger survey.

Methods. We make use of the miniJPAS survey data, conceived as a proof of concept of J-PAS, and covering an area of ≈1 deg^2. Objects were detected in the $r_{\rm SDSS}$ images and selected by imposing a condition on the flux in a given narrow-band J-PAS filter with respect to the contiguous ones, which is analogous to requiring an observed equivalent width larger than 300 Å in a certain emission line within the filter bandwidth. The selected sources were then classified as galaxies or quasi-stellar objects (QSOs) after a comparison of their miniJPAS fluxes with those of a spectral database of objects known to present strong emission lines. This comparison also provided a redshift for each source, which turned out to be consistent with the spectroscopic redshifts when available ($|\Delta z/(1 + z_{\rm spec})| \leq 0.01$).

Results. The selected candidates were found to show a compact appearance in the optical images, some of them even being classified as point-like sources according to their stellarity index. After discarding sources classified as QSOs, a total of 17 sources turned out to exhibit $EW_0 \geq 300$ Å in at least one emission line, thus constituting our final list of EELGs. Our counts are fairly consistent with those of other samples of EELGs in the literature, although there are some differences, which were expected due to biases resulting from different selection criteria.

Key words. galaxies: evolution – galaxies: star formation – galaxies: starburst

1. Introduction

Galaxies dominated by very strong episodes of star formation hold the key to our understanding of the evolution of the Universe; they are the building blocks out of which more massive galaxies are formed (e.g., Ono et al. 2010). They also they might be responsible for a substantial fraction of the UV photon budget required for the re-ionization of the Universe (e.g., Salvaterra et al. 2011; Dressler et al. 2015; Erb et al. 2016; Yang et al. 2017; Sobral et al. 2018a; Naidu et al. 2022; Matthee et al. 2022).

Such galaxies show very intense emission lines, resulting from the ionization of the gas surrounding the young stellar complexes that account for most of the energy radiated away. Depending on the selection method and on their redshifts, extreme emission-line galaxies (EELGs) cover different categories, such as HII galaxies (Terlevich et al. 1991), blue compact dwarf galaxies (BCDs, Kunth & Sargent 1986; Cairós et al. 2001), green pea galaxies (Cardamone et al. 2009; Amorín et al. 2010), blueberry galaxies (Yang et al. 2017), and ELdots (Bekki 2015). Also, several studies report the detection of galaxies with strong emission lines with *Spitzer*/IRAC data using the colour excess in one of the IRAC bands as a proxy for the equivalent width (Labbé et al. 2013; Smit et al. 2015; Castellano et al. 2017; De Barros et al. 2019; Endsley et al. 2021). Some of these objects present intense UV radiation that can double ionize the He, and so they are called HeII emitters (Shirazi & Brinchmann 2012; Cassata et al. 2013; Kehrig et al. 2018). Although such starburst galaxies can be found in the local Universe, they are known to be more frequent at higher redshifts (Endsley et al. 2021; Boyett et al. 2022), where in some cases they can be detected by prominent emission in the Lyα line (e.g., Kunth et al. 2003; Erb et al. 2016; Sobral et al. 2018b; Sobral & Matthee 2019).

Previous works studied EELGs at different redshifts, using a variety of methods: van der Wel et al. (2011) used broad band photometry to select ≈70 EELGs in the CANDELS fields; Amorín et al. (2015) characterized a sample of ≈180 of these galaxies from the 20k zCOSMOS bright survey, at a redshift of $0.11 \leq z \leq 0.93$ selected on the basis of their high EW_0([O[III]); and Maseda et al. (2018) estimated the density of EELGs from an automated line search technique for slitless spectroscopic data from the 3D-HST survey, also based on a high EW_0([O[III]). These studies reveal that EELGs present stellar masses in

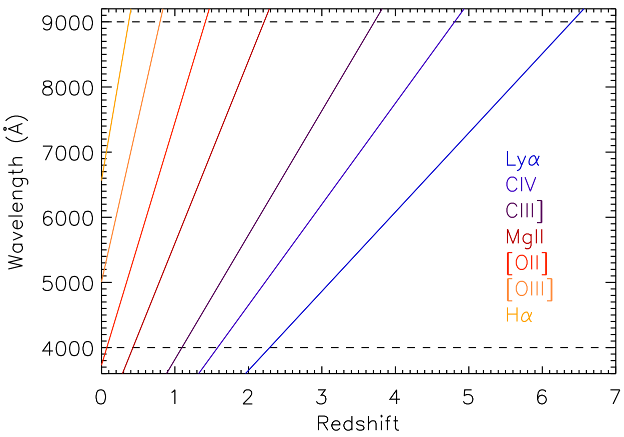

Fig. 1. Wavelength of the most intense emission lines of star-forming galaxies and QSOs as a function of redshift within the wavelength range explored in this work ([4000, 9000]Å).

the range $6.5 \leq \log M^*/M_\odot \lesssim 10$; they are compact, with $r_{50} \lesssim 2$ kpc, and with oxygen abundances 12 + logO/H $\lesssim 8.16$. Khostovan et al. (2016) investigated the properties of a sample of ≈7000 galaxies from the HiZELS survey with strong emission in the Hβ+[OIII] and [OII] emission lines in the redshift range $0.8 \leq z \leq 5$, and found values of the rest-frame equivalent widths in the range $10{-}10^5$ Å.

There is not yet a clear convention on the minimum limiting rest-frame equivalent width (EW_0) to define a galaxy as an EELG; some BCDs show EW_0(Hα) larger than 500 Å (e.g., IZw18, Moustakas & Kennicutt 2006), and typical values of EW_0([OIII]λ5007Å) are larger than 500 Å (e.g., Sobral et al. 2013; Brunker et al. 2020). In general, it is found that the rest-frame EW evolves with redshift as ionization efficiency increases (Sobral et al. 2014; Khostovan et al. 2016). Moreover, Lumbreras-Calle et al. (2021) found a sample of EELGs at $z \leq 0.06$ with [OIII] EW over 300 Å using 2000 deg^2 with the J-PLUS survey (Cenarro et al. 2019).

A complete census of EELGs over a wide redshift range is still an observational challenge. A detailed study of their basic properties at different redshifts is crucial given their relevance as analogous of extreme emitters at high redshift. For this reason, a combination of a wide area survey and an instrumental design sensitive to high equivalent width emission features is an optimal solution to address this problem.

J-PAS, the Javalambre Physics of the Accelerating Universe Survey, will cover ≈8000 deg^2 with 56 contiguous narrow-band (≈120 Å wide) filters, covering from 3800 Å to 9100 Å (Benítez et al. 2009, 2014). The J-PAS design has demonstrated that it is suitable for identifying emission-line galaxies and measuring their fluxes (e.g., Martínez-Solaeche et al. 2021, 2022), and for the characterization of galaxy populations (González Delgado et al. 2021). Moreover, this instrumental setup is optimal for detecting objects with very high flux excess with respect to the contiguous bands.

In this work we consider EELGs as galaxies with $EW_0 \geq$ 300 Å in at least one of the emission lines: [OII]$\lambda\lambda$3727,3729Å (hereafter [OII]), [OIII]λ5007Å (hereafter [OIII]), [OIII]λ4959Å (hereafter [OIII]b), or Hα. As a proof of concept of this project, we tested our method by analysing miniJPAS data (Bonoli et al. 2021), which cover 1 deg^2 overlapping the AEGIS fields, and have the same filter setup and observational strategy as J-PAS. In this regard, this paper describes the method used to detect strong line emitters in the miniJPAS images. Section 2 describes the procedure followed to select EELG candidates and the adopted criteria. Section 3 shows the basic properties of our EELG candidates. In Sect. 4 we discuss some of the statistical results of the EELGs. Finally, Sect. 5 lists the main conclusions of this study and the prospect applicability to the larger J-PAS images.

Throughout this paper we use a flat Λ cold dark matter cosmology, with H_0 = 69.6 km s^{-1}, Ω_0 = 0.286, and Ω_Λ = 0.714 (Bennett et al. 2014).

2. Data and selection procedure

This work makes use of the miniJPAS Public Data Release (miniJPAS-PDR201912[1], December 2019). This survey comprises four AEGIS fields observed with a set of 60 filters in the visible, and covers a total field of view of ≈1 deg^2. A detailed description of the observations, telescope, and instrumental setup is provided in Bonoli et al. (2021).

We define EELGs as objects that show at least one emission line with $EW_0 \geq 300$ Å. From the total J-PAS filter dataset, we only consider the filters covering the wavelength range 4000 Å (filter J0400) to 9000 Å (filter J0900). The reason for this is that the continuum underlying emission lines detected close to the borders of the J-PAS wavelength coverage could be biased, due to the fact that the red or blue sides of the continuum will be under-sampled. As we are interested in detecting star-forming EELGs, the most conspicuous emission lines that satisfy this condition are [OII], [OIII], and Hα. In addition to this, QSOs may also present strong (broad) emission lines in Lyα (1216Å), CIV (1549Å), CIII] (1909Å), and MgII (2800Å).

Figure 1 shows the observed wavelengths of these emission lines as a function of redshift within the wavelength range considered in this work. Our three emission lines of interest ([OII], [OIII], and Hα) are redshifted out of our wavelength range at $z \geq 1.4$, 0.8, and 0.4, respectively. Therefore, our sample contains all EELGs with $EW_0 \geq 300$ Å in [OII], [OIII], and Hα at these redshifts. Nevertheless our sample is not strictly complete since EELGs satisfying our EW_0 criterion in an emission line redshifted out of the [4000, 9000]Å range will never be detected.

The process begins by analysing the information offered by the miniJPAS catalogues issued from Sextractor (Bertin & Arnouts 1996), namely the basic properties of the detections, such as coordinates and fluxes. Sextractor works in two different modes: a single mode (sources are detected and measured on each individual image) and a dual mode (sources are detected in the $r_{\rm SDSS}$ image and measured with the same criteria at the same position on the images corresponding to the rest of the filters). Our starting point will be the dual catalogue that contains the fluxes in all the miniJPAS images of the sources selected and extracted in the $r_{\rm SDSS}$ image. We base our detection procedure in the observable $(F_l - F_c)/F_l$, hereafter denoted as `Contrast`, where F_l is the flux density in the miniJPAS image containing the emission line, and F_c is the flux density of the underlying continuum, derived from the flux densities of the miniJPAS images contiguous to the one containing the emission line. The emission lines of the EELGs are much narrower than the throughput curve of the narrow-band J-PAS filters, so this ensures that all the flux of the emission lines are included in the filter. The `Contrast` is analogous to the observed equivalent width, although more stable for sources with very low continuum levels, as is expected for EELGs. The

[1] http://archive.cefca.es/catalogues/minijpas-pdr201912/

relation between this observable and the observed equivalent width is the following:

$$\frac{F_l - F_c}{F_l} = \frac{EW}{EW + W_n/T_{\mathrm{peak},n}}, \quad (1)$$

where EW corresponds to the observed equivalent width of a given emission feature, W_n is the total area under the throughput curve of filter n containing the emission feature, and $T_{\mathrm{peak},n}$ is the peak throughput of filter n, so that $W_n/T_{\mathrm{peak},n}$ is the effective width of the filter.

As we are interested in galaxies with rest-frame $EW_0 \geq 300$ Å, and EW_0 is always lower than the observed EW, we set a limiting value on the `Contrast` equivalent to observed $EW = 300$ Å. This way, once the redshifts of the candidates is estimated, we keep only those sources with $EW_0 \geq 300$ Å. In order to estimate the limiting value for the `Contrast`, we convolve a synthetic spectrum consisting of a flat continuum and an infinitely narrow emission line with $EW = 300$ Å, with the narrow-band J-PAS filters. The exact value varies slightly from filter to filter, and we adopt an average limiting value of 0.674 for the `Contrast`.

To check the reliability of this method to select EELGs from the miniJPAS data, we first verify that confirmed EELGs are selected in the miniJPAS images using this criterion: for this, we used all the galaxies from SDSS-DR16 (Ahumada et al. 2020) with observed $EW \geq 300$ Å in [OII], [OIII] or Hα present in the miniJPAS images. EWs were measured by fitting the SDSS spectra to Gaussian functions. A total of 0/6/1 galaxies were found to present observed $EW \geq 300$ Å in [OII]/[OIII]/Hα. For each of these galaxies, we derived the `Contrast` from the miniJPAS data in the following way: F_l was taken to be the flux density measured in the narrow-band filter n, whose central wavelength is closer to that of the emission line. F_c was estimated by a linear fitting of the flux densities from the dual catalogue corresponding to the filters with $100\,\text{Å} \leq |\lambda_i^{\mathrm{cen}} - \lambda_n^{\mathrm{cen}}| \leq 1000\,\text{Å}$[2], where λ_i^{cen} is the central wavelength of filter i, interpolating the fit at the central wavelength of the filter. Given the faint nature of these objects, 2000 Å is a reasonable baseline to define a stable continuum flux. In the case of the Hα line, the continuum is estimated in the (rest-frame) spectral region $5563\,\text{Å} \leq \lambda \leq 7563\,\text{Å}$, excluding the filter containing Hα and the two adjacent ones. The brightest emission lines in this spectral region are those of [SII]$\lambda\lambda$6717, 6731 Å, which are much fainter than Hα. In the case of the [OIII] line, the continuum is estimated in the (rest-frame) spectral range $4007\,\text{Å} \leq \lambda \leq 6007\,\text{Å}$, excluding the filter containing the [OIII] line, and the two adjacent ones (that contain the [OIII]b and Hβ lines), and there are no other bright lines in the spectral range used to estimate the continuum. Finally, the case of the [OII] lines is similar to the previous cases. There are several emission lines in the spectral range selected to estimate the continuum but they are much fainter than the [OII] lines. In the three cases, there are no bright emission lines in the wavelength range used to estimate the continuum, and thus we are confident that the value derived for the continuum is not biased.

In addition, we also derived from the miniJPAS data, the continuum flux density underlying the emission line ($f_{c,l}$), and the flux of the emission line (F_λ). $f_{c,l}$ was derived in a similar way as F_c but interpolating the fit at the wavelength of the emission line. F_λ was estimated by deconvolving F_l with the profile of the filter n, assuming a value of $f_{c,l}$ for the continuum flux density, and that the emission line is infinitely narrow. To derive these quantities, we used the Sextractor AUTO magnitudes. The uncertainties of these quantities were derived by producing 1000 random realizations of the J-spectra[3] of each source, assuming that the uncertainties of the fluxes are Gaussian. The final adopted uncertainties are then half the difference of the percentiles 15.9 and 84.1 of the 1000 derived values of each quantity.

In Fig. 2 we show a comparison of the parameters of the emission lines as derived from the miniJPAS data, compared to the same quantities measured from the SDSS spectra. The top panel shows the observed EWs measured from the SDSS spectra, as a function of the `Contrast` estimated from the miniJPAS data. As expected, the `Contrast` measured for these sources is larger than the limiting value 0.674, which supports the use of this threshold to identify EELGs. In addition to this, the middle panel shows the flux estimated from the miniJPAS fluxes (F_λ) as a function of the flux of the emission lines measured from the SDSS spectra. As it can be seen, the agreement is good, although the fluxes derived from the miniJPAS data for the most intense emission lines are slightly underestimated (≈10%) compared to the SDSS values. This discrepancy could be due to the fact that the SDSS fibre does not include all the flux that we measure in the miniJPAS image. Finally, the bottom panel shows the continuum flux density at the base of the emission lines derived from the miniJPAS data as a function of the same quantity measured from the SDSS spectra. In this case, the agreement is fair for the lowest continuum levels, and again the values estimated from the miniJPAS data are below the values derived from the SDSS spectra. Only one of the galaxies shows important differences in the derived values of the continuum and the equivalent width when we compare the SDSS and miniJPAS data. This galaxy was selected in the Hα line and its redshift places this line at ≈7930 Å, where the sky lines start to significantly contaminate the observational data. This, together with the fact that the continuum of this galaxy is quite low, and that the AUTO photometry could not match the same aperture of the SDSS fibre, might explain the disagreement between the continuum values from SDSS and miniJPAS. However, the remaining galaxies show a reasonable agreement, suggesting that this method is useful for selecting EELGs from the miniJPAS images. We detail below the steps followed to produce our list of EELG candidates.

As previously explained, we base our selection on the miniJPAS dual catalogue containing objects selected and extracted in the r_{SDSS} image. It should be noted that this introduces a bias in the sense that EELGs not detected in the r_{SDSS} image will not be selected even if they fulfil the rest of the conditions described below. We comment on this point latter in the paper. For each of the narrow-band J-PAS filters of interest to us (from J0400 to J0900), n, we select from the corresponding dual catalogue[4], all sources fulfilling the following criteria: (a) $F_n \geq 10^{-17}$ erg s^{-1} cm^{-2} Å^{-1}, where F_n is the flux density of the source in filter n; (b) FLAG ≤ 3 and MASK_FLAG ≤ 0, to avoid uncertainties derived from instrumental artefacts and false detections[5]; (c) $F_{8500}/F_{4300} < 1.2$, to avoid spurious detections of red objects, where F_{8500} is the median of the flux in the filters [J0800, ..., J0900] and F_{4300} is the median of the flux in the filters [J0378, ..., J0480]; and (d) having a counterpart in the single

[2] This condition excludes filter n and its two contiguous filters from the fit. This way, we avoid flux densities corresponding to the filters that could be contaminated by the emission line.

[3] A J-spectra is defined as the low-resolution ($R \approx 60$) spectrum composed by the fluxes of an object in all the J-PAS filters (Bonoli et al. 2021).

[4] *minijpas.FLambdaDualObj* in the miniJPAS database.

[5] FLAG and MASK_FLAG values defined in `http://archive.cefca.es/catalogues/minijpas-pdr201912/help_adql.html`

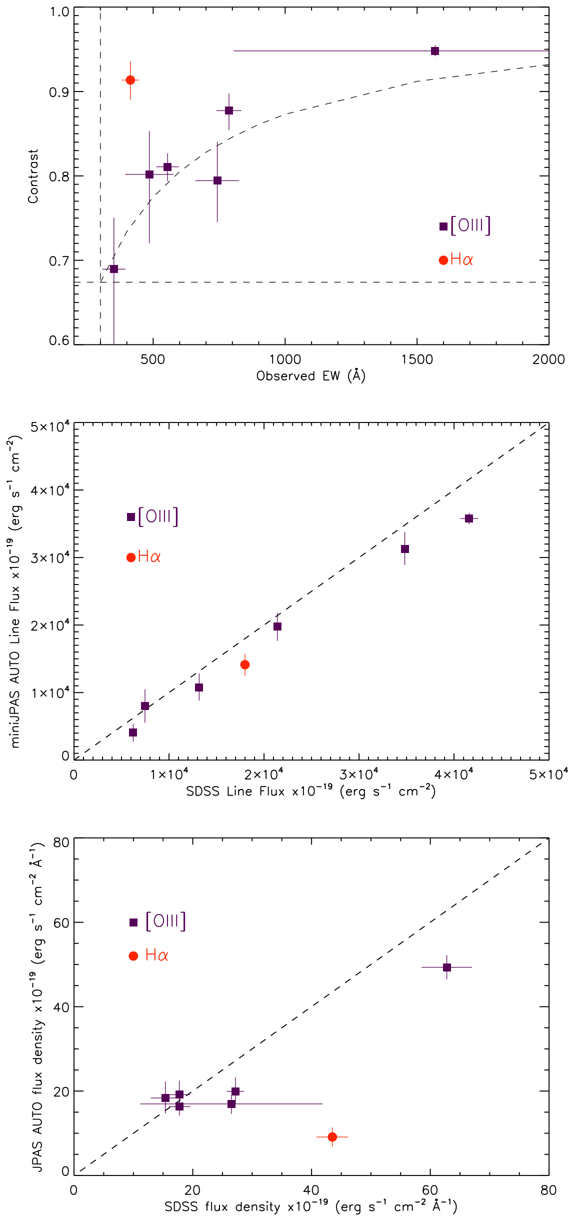

Fig. 2. Comparison of quantities derived from miniJPAS data and from the SDSS spectra. *Top*: contrast derived from the miniJPAS data as a function of the observed EW measured from the SDSS spectra for the SDSS galaxies showing emission lines with observed EW larger than 300 Å. The vertical and horizontal dashed lines correspond to our lower limits in the observed EW and the Contrast, respectively. The curved dashed line corresponds to the theoretical relation between the observed EW and the `Contrast`. *Middle*: emission line fluxes derived from the miniJPAS data as a function of the fluxes measured from the SDSS spectra. The dashed line corresponds to the one-to-one relation. *Bottom*: continuum flux densities derived from the miniJPAS data as a function of the continuum flux densities measured from the SDSS spectra. The dashed line corresponds to the one-to-one relation.

catalogue[6] corresponding to filter n, to ensure a real detection in the miniJPAS images.

For each of these selected sources, we estimate a continuum flux density, F_c. For this, we follow the same procedure that was previously explained for the SDSS galaxies.

Finally, we impose the condition of minimum `Contrast` $(F_n - F_c)/F_n \geq 0.674$, corresponding to observed $EW \geq 300$ Å in at least one emission feature, to confirm the source as an EELG candidate. As the rest-frame EW_0 is always lower than the observed EW, once the redshifts of the candidates are estimated, some of the selected sources are discarded if their EW_0 is lower than our limiting value of 300 Å.

A visual inspection of the EELG candidates suggests the need to add one further condition to remove undesirable detections: objects whose intensity peak in filter n is lower than $5 \times \sigma$, where σ is the standard deviation of the sky of the corresponding image n, are discarded since they are too noisy and produce spurious detections.

We did not impose any condition on the stellarity index of the selected sources since EELGs are known to show a compact appearance (e.g., Amorín et al. 2015), and thus they could be misclassified as stars in the optical images. Thus, we end up with a list of 43 EELG candidates, corresponding to 31 different sources since nine of them were detected in more than one filter.

As previously stated, our sample is very likely contaminated by high-redshift QSOs. In order to disentangle the nature of our candidates (star-forming galaxy or QSO), we fitted their J-spectra to those of a sample of star-forming galaxies and QSOs with SDSS spectroscopy in DR16. The SDSS spectra cover most of the J-PAS wavelength range, so they are ideal for comparing to the miniJPAS data. SDSS QSO and star-forming spectra were extracted from the SDSS-DR16 database and selected on the basis of their prominent emission lines (according to Thomas et al. 2013). All these SDSS spectra, as well as the SDSS pipeline best-model fits used for classification and redshift, were shifted from $z - 0.05$ to $z + 0.05$ in steps of 0.002, to continuously cover a wide redshift range up to $z = 1.4$ for star-forming galaxies, and up to $z = 6.49$ for QSOs. Finally, synthetic photometry of these spectra was performed in the narrow-band J-PAS filters, thus constituting our comparison database of J-spectra. In addition to this set of real spectra, our comparison database was completed with a set of synthetic spectra that was artificially generated. For this we used two continua (in the wavelength interval [3700, 9000]Å) typical of strong star-forming galaxies, and we superposed narrow emission lines ([OII], Hβ, [OIII], [OIII]b, and Hα), filling the areas designed by the relations shown in Fig. 3. This figure shows the relations between EW_0 of [OII], [OIII], and Hα for our sample of star-forming SDSS spectra. These synthetic spectra were also convolved with the J-PAS filters and the results were included in our comparison database of J-spectra.

For each candidate, its J-spectra were compared to all the J-spectra present in our database, and were assigned to a χ^2 value. The final redshift and QSO or galaxy classification adopted for each candidate are those corresponding to the spectrum with the minimum χ^2.

The result of this fitting procedure yielded 20 (64.5%) star-forming galaxies from the EELG candidates, and 11 (35.5%) QSOs. As a way of checking the consistency of our classification, compared to other ways of identifying QSOs, we searched whether our sources have X-ray counterparts. Only six of our candidates were found to be X-ray sources in NED[7], and all of them were classified as QSOs.

[6] *minijpas.FLambdaSingleObj* in the miniJPAS database.

[7] The NASA/IPAC Extragalactic Database (NED) is operated by the Jet Propulsion Laboratory, California Institute of Technology, under contract with the National Aeronautics and Space Administration.

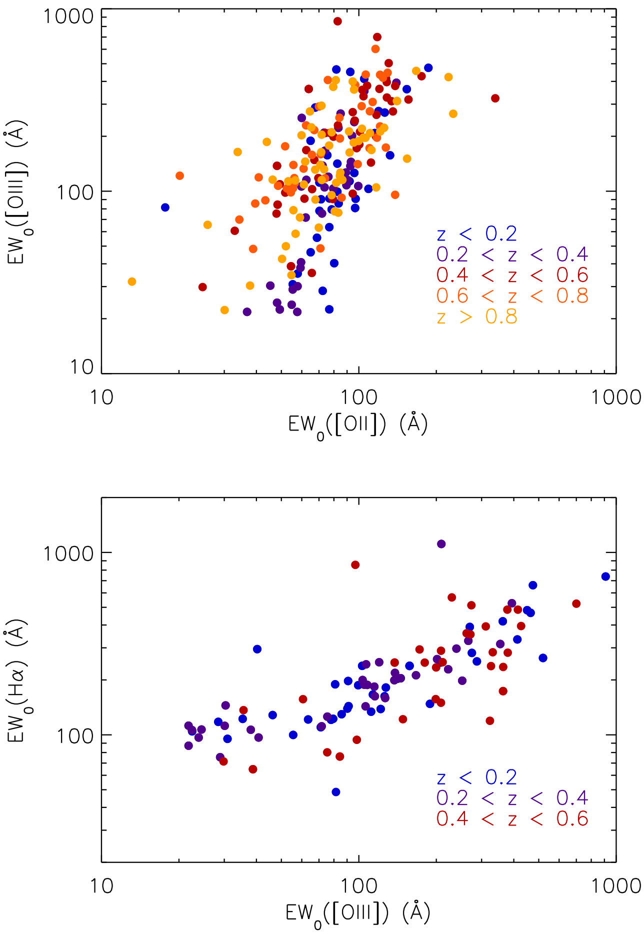

Fig. 3. Comparison of the EWs of different emission lines for a sample of strong emission-line galaxies from SDSS. *Top*: EW_0([OII]) as a function of EW_0([OIII]). *Bottom*: EW_0([OIII]) as a function of EW_0(Hα).

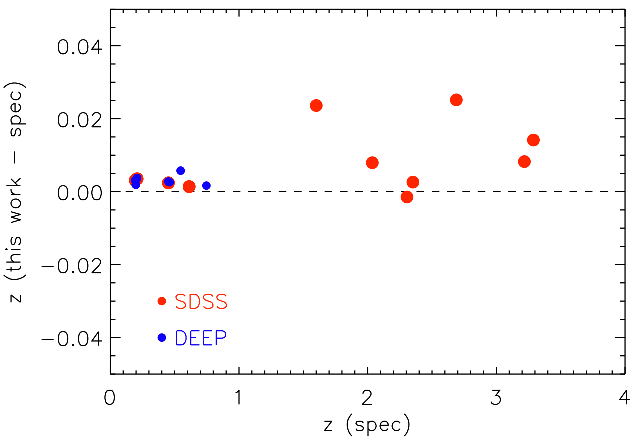

Fig. 4. Redshift difference as a function of the spectroscopic redshifts from SDSS (red) and DEEP2/3 (blue) for the EELG candidates present in the SDSS and DEEP databases.

3. Properties of the selected candidates

Table B.1 shows the basic properties of our detected sources. These include: quantities extracted from the J-PAS catalogues, such as coordinates, magnitude, and stellarity index; quantities derived in this work such, as redshift, rest-frame equivalent width, flux, and luminosity of the detected emission lines; and spectroscopic redshifts from SDSS and DEEP2 or DEEP3 when

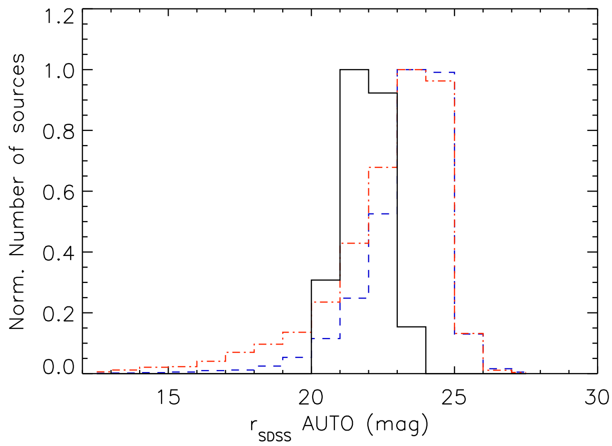

Fig. 5. Histogram of the $r_{\rm SDSS}$ (AUTO photometry) magnitude of our selected candidates (black line). Blue and red histograms correspond to the total sample of galaxies and stars in the miniJPAS dual catalogue, respectively, classified taking into account the miniJPAS stellarity index. The three histograms are normalized to the peak of each distribution.

available. Rest-frame equivalent widths were derived using our z estimation for all sources, to keep consistency with the whole sample.

With these SDSS and DEEP spectroscopic redshifts, we can estimate the goodness of our methodology and the precision of the derived redshifts, which are relevant for the subsequent analysis based on the luminosities of the brightest emission lines of our candidates. A cross-match within a 1″ radius results in 11 objects from our list having available spectroscopic redshifts in SDSS, and seven objects in DEEP2 or DEEP3; this gives a total of 15 objects having a spectroscopic redshift in at least one of these three catalogues. A comparison of the redshifts derived in this work with the spectroscopic redshifts is shown in Fig. 4. All the redshifts derived in this work are consistent with the corresponding spectroscopic redshifts, to a level that allows us to unequivocally identify the emission line that was selected as extreme. The most deviant points are those corresponding to redshifts larger than one, which are classified as QSOs. For all the sources we find $|\Delta z/(1 + z_{\rm spec})| \leq 0.01$. We point out that our aim is not to make a detailed redshift analysis, since the methodology followed to select EELGs is not optimized to derive photometric redshifts. Our only interest is to derive redshifts consistent with the spectroscopic redshifts in order to be able to identify the emission line detected by our method, and estimate fluxes, luminosities, and rest-frame equivalent widths with reasonable accuracy. Hereupon, our methodology has proven to reach the necessary accuracy, although misidentification may still occur on a few occasions in a larger sample.

Figure 5 shows the histogram of the $r_{\rm SDSS}$ magnitude with the AUTO photometry for the selected objects. The peak of the detections ranges from 21 to 22 mag, the majority of them being in the range 20–23 mag. The magnitude range covered by our sample shows the intrinsic difficulty to identify these objects in broad-band photometric surveys, compared to samples of other types of galaxies. As it is shown in Table B.1, some of the star-forming candidates are classified as stars in the miniJPAS catalogues based on the miniJPAS stellarity indices. In the case of the QSOs, all but one are classified as stars based on the same index. Figure A.1 shows the images of the candidates in the filter where they were detected, and it shows that most of them show a compact appearance.

4. The confirmed EELGs

As explained in Sect. 2, our selected candidates present observed $EW \geq 300$ Å in at least one emission feature. Nevertheless, we consider only those candidates classified as galaxies and showing $EW_0 \geq 300$ Å as confirmed EELGs. To estimate their EW_0s, the first step is to recover the fluxes of the brightest emission lines of our EELG candidates. We note that the partial overlap of some contiguous J-PAS filters might result, for some galaxies, in multiple detections of the same emission line in different filters. On the other hand, more than one emission line could be detected by the same J-PAS filter, depending on the redshift of the source. This is particularly frequent in the case of Hβ, [OIII]b, and [OIII], since these three lines are in close proximity to each other. It is even more frequent in the case of [NII]λ6548Å, Hα, [NII]λ6583Å. However, the intensities of the [NII] lines are expected to be much fainter than the Hα line, so that as a first approximation, we assumed a mean line ratio of [NII]λ6583Å/Hα = 0.05 for all the galaxies, which is considered typical for galaxies with strong emission lines (e.g., Pérez-Montero et al. 2011; Amorín et al. 2012; Kehrig et al. 2020).

Table B.1 contains the EW_0 values, fluxes, and luminosities of the selected emission features of the EELG candidates, derived from the AUTO J-spectra. The emission line fluxes were derived from the miniJPAS fluxes, assuming an infinitely narrow emission line at the derived redshift, so that the filter (or filters) where the emission line is detected contains (contain) all the flux from the line. This approximation is reasonable for star-forming galaxies, although it does not necessarily hold for QSOs; their emission lines in the rest-frame UV, which shift into the optical at the redshifts where we are detecting them, are mostly broad. For this reason, the derived values of EW_0, fluxes, and luminosities of the QSO emission lines quoted in Table B.1 are approximations that could have significant associated uncertainties.

A total of 17 sources that satisfy our criterion on the $EW_0 \geq 300$ Å are classified as star-forming galaxies, and thus they can be considered as confirmed EELGs. Of these, 12 are extreme emitters in [OIII], two in Hα, and three in both [OIII] and Hα. It is important to note that in our sample, we do not find EELGs selected in the [OII] line. In fact, such galaxies are rare up to high redshifts (Darvish et al. 2015; Cava et al. 2015; Reddy et al. 2018; Cedrés et al. 2021), although they do exist. Thus, even if they are absent in our small sample, some of them should be detected in the whole J-PAS survey.

4.1. Investigating contamination due to Lyα emitters

In this section we discuss whether some of our confirmed EELGs could be high-redshift Lyα emitters misclassified as lower redshift star-forming galaxies. This might happen if some of the redshifts of the sources with no spectroscopic counterparts are not correctly estimated. Lyα emitters have already been detected in the J-PLUS survey (Cenarro et al. 2019) in the redshift range $2.2 \leq z \leq 3.3$ (Spinoso et al. 2020). If any of these star-forming Lyα emitters were present in the miniJPAS images, it would be misclassified since our spectral database used to disentangle between galaxies and QSOs does not include spectra of star-forming galaxies at $z \geq 1.4$. This not the case for QSOs, since these objects are represented in our database and are properly classified (see Table B.1).

The rest-frame UV spectra of star-forming Lyα emitters show a quite flat and usually faint continuum, a Lyα line with a high equivalent width (≥50 Å), and several other lines with lower intensity such as CIVλ1550Å, HeIIλ1640Å, OIII]$\lambda\lambda$1661, 1667Å, and CIII]λ1909Å (e.g., Verhamme et al. 2017; Nakajima et al. 2018; Feltre et al. 2020). This means that the J-spectra of a high-redshift, star-forming, Lyα-emitting galaxy would show a flat and faint continuum with a peak in one of the narrow-band filters due to the presence of the Lyα line. A detailed look at the J-spectra of our selected sample, shown in Fig. A.1, shows that this is the case for several of them, although they are classified as [OIII] or Hα emitters. This raises the question of whether they could be misclassified star-forming Lyα emitters.

In order to disentangle the two possibilities, we make use of the information available in the literature. If we assume that all our confirmed EELGs are indeed high-redshift Lyα galaxies, the detected emission line would be Lyα, and their redshift range would be $2.30 \leq z \leq 6.20$. In addition, their Lyα luminosities would be in the range $43.79 \leq \log L_{\mathrm{Ly}\alpha}/(\mathrm{erg\,s^{-1}}) \leq 44.93$, and their corresponding rest-frame absolute UV magnitudes averaged over [1000, 2000]Å would be in the range $-25.19 \leq M_{\mathrm{UV,AB}} \leq -21.92$[8]. The values of these rest-frame UV magnitudes and Lyα luminosities are much brighter than expected at such high redshifts (Khusanova et al. 2020). Also, regarding the Lyα luminosities, Sobral et al. (2018b) suggest that these values of Lyα luminosity correspond to the high-luminosity end of the Lyα luminosity function (evaluated between $2.5 \leq z \leq 6$) and that they would be scarce, and thus hard to detect in a 1 deg^2 survey. In addition to this, such high luminosities are usually associated with QSOs, whose Lyα emission is related to active galactic nucleus activity. In fact, most QSOs detected in this work show derived Lyα luminosities in this range, as is shown in Table B.1. Moreover, as mentioned in Sect. 2, six of our sources show X-ray emission and all of them are classified as QSOs, as expected for their luminosities if their selected line was Lyα. Bearing in mind that our redshift detection algorithm is not infallible, which might result in some misclassification, the aforementioned reasons support the conviction that our sample of confirmed EELGs is not dominated by star-forming galaxies with strong Lyα-emission redshift into the visible range of the spectrum. In fact, star-forming Lyα emitters fulfilling our requirement in EW_0 have been reported (Malhotra & Rhoads 2002; Kerutt et al. 2022). Thus, although they are absent in our sample, they are expected in the total J-PAS survey and could constitute a source of confusion with EELGs at lower redshifts.

4.2. The Hα and [OIII] luminosity functions

An interesting point to be discussed is the estimation of the range of luminosities that will be observed by J-PAS. For this, we compare the luminosities of our confirmed EELGs to the luminosity functions (LFs) reported by Comparat et al. (2016) for the [OIII] and Hβ lines, at different redshifts. These LFs correspond to galaxies with emission lines and are not restricted to EELGs; we use them because they cover our redshift range and they are useful to illustrate the variation with redshift of the depth of our sample compared to the values of $L*$. These authors derived the LFs of these lines and report the values of the parameters as a function of redshift. In particular, for our comparison we use the parameters derived from the fit of the LF using a Schechter function (Schechter 1976). Figure 6 shows the evolution of the

[8] The values of the absolute UV magnitudes and Lyα luminosities have been derived assuming that the detected emission line is Lyα, and estimating rest-frame UV continua and line luminosity from the observed J-spectra.

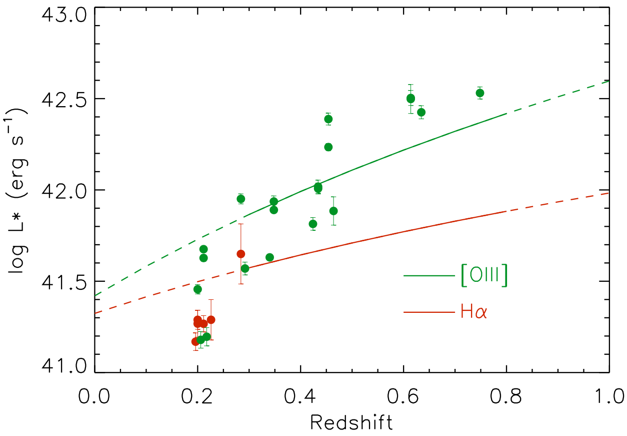

Fig. 6. Evolution of the characteristic luminosity $L*$ as a function of redshift, according to Comparat et al. (2016) for the [OIII]λ5007Å (solid green) and Hα (solid red) lines. The dashed lines are the extrapolations for redshifts out of the ranges where the values of $L*$ of each line were estimated. Filled points correspond to our confirmed EELGs, with the same colour code.

characteristic luminosity $L*$ of the LFs with redshift. As some of our objects were detected in the Hα line, we modified the LF for Hβ given by Comparat et al. (2016) into Hα assuming a constant ratio of Hα/Hβ =2.78. As it can be seen, for EELGs detected in the [OIII] line, we are sensitive to luminosities even lower than $L*$ at redshifts $z \leq 0.5$. In the case of EELGs detected in Hα, the same holds for redshifts $z \leq 0.25$. Otherwise, we only detect galaxies more luminous than $L*$ in both lines. In summary, J-PAS will allow us to probe the low-luminosity regime of the LF for the Hα and [OIII] lines at redshifts lower than 0.25 and 0.5, respectively, assuming that it will be as deep as miniJPAS at detecting EELGs. Importantly, it will provide relevant information on the high-luminosity end of the LF of these emission lines at higher redshifts.

4.3. Number density of EELGs

In this section we address the point of the number of detected EELGs compared to reported densities of similar objects in the literature. A detailed comparison is not simple since the different samples are selected by applying different conditions and from photometric samples with different biases.

As previously mentioned, our sample uses the dual catalogue produced by Sextractor, which means that it takes into account only sources selected in the $r_{\rm SDSS}$ images. In addition to this, we impose a further condition on the flux in the narrow-band filter where the galaxies are selected. These two conditions result in a bias in the sense that galaxies fainter than a given $r_{\rm SDSS}$ magnitude, whose flux is lower than our limit (10^{-17} erg s^{-1} cm^{-2}), will not be detected. Quantifying this bias is not a simple question since our galaxies are detected in a very wide range of wavelengths, and the $r_{\rm SDSS}$ magnitude mimics the continuum at wavelengths in the range [6000, 7000]Å. A first estimation for these subset of galaxies means that we start to be incomplete at magnitudes fainter than $r_{\rm SDSS} \approx 22.3$, and this number could vary for galaxies detected at different wavelengths. In order to get an idea of the completeness of our sample, we compare with samples of similar objects selected with different criteria.

Cardamone et al. (2009) reported a spatial density of Green Peas of $\approx$2 deg^{-2}, imposing conditions on $r_{\rm SDSS}$, redshift, optical colours, and morphology. A comparison with our sample is difficult due to biases induced by the different conditions imposed. In particular, our sample contains galaxies much fainter than those of Cardamone et al. (2009). Only one of our galaxies presents properties close to compatible with the sample of Cardamone et al. (2009)[9], which suggests that our counts are consistent with those of the Green Peas.

In the very local Universe, Yang et al. (2017), in their study of blueberries – that is Green Peas with $z \leq 0.05$ and EW_0([OIII]) $\geq$ 800 Å – reported a total of 43 objects in 14 555 deg^2, which gives a total of $\approx$0.003 deg^{-2}. Also, Lumbreras-Calle et al. (2021) found 466 EELGs in 2000 deg^2 with $z \leq 0.06$ and $EW_0 \geq$ 300 Å in the J-PLUS survey. Our results are consistent with these two works since we find no detections at these redshift ranges.

A more complete study on the number density of EELGs was performed by Amorín et al. (2015) using spectroscopic data from the zCOSMOS-bright survey, covering $\approx$1.7 deg^{-2}. These authors used the 20k-bright sample, which consists of 20 000 galaxies with spectroscopic spectra at $z \leq 2$, down to $I_{\rm AB} \leq 22.5$ as measured from the HST-ACS imaging. They reported a number of 165 EELGs with EW_0([OIII]) $\geq$ 100 Å, in the redshift range $0.11 \leq z \leq 0.93$. The upper limit of this redshift range is above the limit where the [OIII] line is not visible in the J-PAS data ($z \approx 0.8$). Also their limit of EW_0([OIII]) $\geq$ 100 Å is below our limit for considering EELGs. For these reasons, we made use of their Fig. 3 to estimate the number of their galaxies satisfying our condition in $EW_0 \geq$ 300 Å, and within the redshift range $0.11 \leq z \leq 0.8$, which is a range of redshift compatible with the limits of our work and that of Amorín et al. (2015), resulting in a total of 37 galaxies. Taking into account the area surveyed in this work, this corresponds to a density of 21.7 deg^{-2}. Our sample contains 15 EELGs with $EW_0 \geq 300$ in the [OIII] line, and within the redshift range $0.11 \leq z \leq 0.8$, which is slightly below the estimations of Amorín et al. (2015). As we have previously mentioned, the observed discrepancy on the estimated EELG densities by means of different samples could be explained in terms of the different selection criteria imposed by methodology. In fact, Amorín et al. (2015) find a similar quantity of EELGs along the whole redshift range probed (i.e. up to $z = 0.9$), whereas we only select EELGs in [OIII] in the redshift range $0.206 \leq z \leq 0.748$, even when our observational limits allow us to detect them below $z \leq 0.8$. This difference might result from a limitation of the miniJPAS data, an effect of small statistics, or cosmic variance, which can be properly addressed by means of larger samples.

To summarize, precise comparisons with other samples of similar objects are prevented by the different selection criteria of each sample. But even in this case, we find numbers fairly consistent (slightly lower in some cases) with the reported counts of other samples of EELGs.

5. Conclusions

We performed a search of EELGs with the miniJPAS data, covering 1 deg^2, based on a method using the `Contrast` of the emission in one of the J-PAS narrow-band filters with respect to the continuum derived from the contiguous filters. EELGs were selected from the miniJPAS catalogue of sources selected in the $r_{\rm SDSS}$ images. We define EELGs as galaxies that exhibit $EW_0 \geq$ 300 Å in at least one of the emission lines [OII], [OIII],

[9] $r_{\rm SDSS}$ = 20.8, whereas Cardamone et al. (2009) considers galaxies with $18 \leq r_{\rm SDSS} \leq 20.5$.

or Hα. The method used to select our candidates imposed a minimum `Contrast` that corresponds to an observed $EW \geq 300$ Å. 43 emission-line candidates corresponding to 31 sources satisfying this criterion were selected.

We used a database of SDSS-DR16 spectra to derive redshifts for our sources and to classify them as star-forming galaxies or QSOs. The comparison of the J-spectra with the SDSS spectra resulted in 20 of our sources being star-forming EELG candidates, and the remaining 11 sources are classified as QSOs. In addition, the redshifts derived for our sources are in good agreement with the spectroscopic redshifts: after comparing with the spectroscopic redshifts that are available from SDSS and DEEP2/3, all of the 15 objects with available spectroscopic redshift were assigned a proper redshift from their J-spectra. For all the sources we found $\Delta z/(1 + z_{\rm spec}) \leq 0.01$.

Most of the star-forming EELG candidates were detected in the [OIII] line, some of them were detected in the Hα line, and none of them were detected in the [OII] line. In the case of the QSOs, most of them were detected in the Lyα line, and two of them in the CIV line.

Finally, 17 candidates are classified as star-forming galaxies, satisfying the condition of minimum rest-frame EW_0 in Hα or [OIII], and constitute our list of confirmed EELGs. They were detected in the redshift range $0 \leq z \leq 0.748$, with a peak corresponding to the distribution of the [OIII] sources at $0.2 \leq z \leq 0.3$.

Assuming that J-PAS will be as deep as miniJPAS, it will be able to probe the bright end of the Hα and [OIII] luminosity functions of EELGs at redshifts larger than 0.25 and 0.5, respectively. In addition, EELGs with Hα and [OIII] luminosities lower than the corresponding $L*$ will be accessible for J-PAS at lower redshifts.

Although strict comparisons with other samples are difficult due to the different imposed selection criteria, we find a fair agreement in the counts of our sample compared to the EELGs of Cardamone et al. (2009), Yang et al. (2017), and Lumbreras-Calle et al. (2021). Our counts are, however, slightly lower than those of Amorín et al. (2015) who used the zCOSMOS data, but still within the uncertainties.

Our small sample prevents a more detailed study on the basic properties of EELGs. However, this work can be regarded as a successful pilot study, demonstrating the diagnostic power of the presented methodology to detect strong emission-line galaxies. The ongoing J-PAS survey, covering $\approx$8000 deg^2, will result in a much larger sample as it is expected to detect a considerable number of such galaxies, including [OII] emitters, which were absent in the miniJPAS sample due to its small size, and will allow to the nature and evolution of EELGs to be unveiled.

In the interest of supplementing this study and performing a thorough evaluation of this method, a spectroscopic follow-up of this sample is required. This will allow us to estimate the fraction of inaccurate detections (if any), and to crosscheck the accuracy of the emission-line fluxes estimated from the miniJPAS data.

Acknowledgements. This work has been partially funded by projects PID2019-107408GB-C44 from the Spanish PNAYA, co-funded with FEDER, and grand P18-FR-2664, funded by Junta de Andalucía. We acknowledge financial support from the State Agency for Research of the Spanish MCIU through the "Center of Excellence Severo Ochoa" award to the Instituto de Astrofísica de Andalucía (SEV-2017-0709). RGD and LADG acknowledge financial support from the State Agency for Research of the Spanish MCIU through the "Center of Excellence Severo Ochoa" award to the Instituto de Astrofísica de Andalucía (SEV-2017-0709), and PID2019-109067-GB100. IM acknowledges financial support from the State Agency for Research of the Spanish MCIU through the PID2019-106027GB-C41. JCM acknowledges partial support from the Spanish Ministry of Science, Innovation and Universities (MCIU/AEI/FEDER, UE) through the grant PGC2018-097585-B-C22. SDP is grateful to the Fonds de Recherche du Québec – Nature et Technologies. LSJ acknowledges the support of CNPq (304819/2017-4) and FAPESP (2019/10923-5). JAFO acknowledges the financial support from the Spanish Ministry of Science and Innovation and the European Union – NextGenerationEU through the Recovery and Resilience Facility project ICTS-MRR-2021-03- CEFCA. Funding for the J-PAS Project has been provided by the Governments of España and Aragón though the Fondo de Inversión de Teruel, European FEDER funding and the MINECO and by the Brazilian agencies FINEP, FAPESP, FAPERJ and by the National Observatory of Brazil. Based on observations made with the JST/T250 telescope and PathFinder camera for the miniJPAS project at the Observatorio Astrofísico de Javalambre (OAJ), in Teruel, owned, managed, and operated by the Centro de Estudios de Física del Cosmos de Aragón (CEFCA). We acknowledge the OAJ Data Processing and Archiving Unit (UPAD) for reducing and calibrating the OAJ data used in this work. Funding for OAJ, UPAD, and CEFCA has been provided by the Governments of Spain and Aragón through the Fondo de Inversiones de Teruel; the Aragón Government through the Research Groups E96, E103, and E16_17R; the Spanish Ministry of Science, Innovation and Universities (MCIU/AEI/FEDER, UE) with grant PGC2018-097585-B-C21; the Spanish Ministry of Economy and Competitiveness (MINECO/FEDER, UE) under AYA2015-66211-C2-1-P, AYA2015-66211-C2-2, AYA2012-30789, and ICTS-2009-14; and European FEDER funding (FCDD10-4E-867, FCDD13-4E-2685). This research has made use of the NASA/IPAC Extragalactic Database (NED), which is operated by the Jet Propulsion Laboratory, California Institute of Technology, under contract with the National Aeronautics and Space Administration. Funding for SDSS-IV has been provided by the Alfred P. Sloan Foundation, the Participating Institutions, the National Science Foundation, and the U.S. Department of Energy Office of Science. The SDSS-IV web site is https://www.sdss.org/. This project has received funding from the European Union's Horizon 2020 research and innovation programme under the Marie Sklodowska-Curie grant agreement No 898633.

References

Ahumada, R., Prieto, C. A., Almeida, A., et al. 2020, ApJS, 249, 3
Amorín, R. O., Pérez-Montero, E., & Vílchez, J. M. 2010, ApJ, 715, L128
Amorín, R., Pérez-Montero, E., Vílchez, J. M., et al. 2012, ApJ, 749, 185
Amorín, R., Pérez-Montero, E., Contini, T., et al. 2015, A&A, 578, A105
Bekki, K. 2015, MNRAS, 454, L41
Benítez, N., Moles, M., Aguerri, J. A. L., et al. 2009, ApJ, 692, L5
Benítez, N., Dupke, R., Moles, M., et al. 2014, ArXiv e-prints [arXiv:1403.5237]
Bennett, C. L., Larson, D., Weiland, J. L., et al. 2014, ApJ, 794, 135
Bertin, E., & Arnouts, S. 1996, A&AS, 117, 393
Bonoli, S., Marín-Franch, A., Varela, J., et al. 2021, A&A, 653, A31
Boyett, K. N. K., Stark, D. P., Bunker, A. J., et al. 2022, MNRAS, 513, 4451
Brunker, S. W., Salzer, J. J., Janowiecki, S., et al. 2020, ApJ, 898, 68
Cairós, L. M., Vílchez, J. M., González Pérez, J. N., et al. 2001, ApJS, 133, 321
Cardamone, C., Schawinski, K., Sarzi, M., et al. 2009, MNRAS, 399, 1191
Cassata, P., Le Fèvre, O., Charlot, S., et al. 2013, A&A, 556, A68
Castellano, M., Pentericci, L., Fontana, A., et al. 2017, ApJ, 839, 73
Cava, A., Pérez-González, P. G., Eliche-Moral, M. C., et al. 2015, ApJ, 812, 155
Cedrés, B., Bongiovanni, Á., Cerviño, M., et al. 2021, A&A, 649, A73
Cenarro, A. J., Moles, M., Cristóbal-Hornillos, D., et al. 2019, A&A, 622, A176
Comparat, J., Zhu, G., Gonzalez-Perez, V., et al. 2016, MNRAS, 461, 1076
Darvish, B., Mobasher, B., Sobral, D., et al. 2015, ApJ, 814, 84
De Barros, S., Oesch, P. A., Labbé, I., et al. 2019, MNRAS, 489, 2355
Dressler, A., Henry, A., Martin, C. L., et al. 2015, ApJ, 806, 19
Endsley, R., Stark, D. P., Chevallard, J., et al. 2021, MNRAS, 500, 5229
Erb, D. K., Pettini, M., Steidel, C. C., et al. 2016, ApJ, 830, 52
Feltre, A., Maseda, M. V., Bacon, R., et al. 2020, A&A, 641, A118
González Delgado, R. M., Díaz-García, L. A., de Amorim, A., et al. 2021, A&A, 649, A79
Kehrig, C., Vílchez, J. M., Guerrero, M. A., et al. 2018, MNRAS, 480, 1081
Kehrig, C., Iglesias-Páramo, J., Vílchez, J. M., et al. 2020, MNRAS, 498, 1638
Kerutt, J., Wisotzki, L., Verhamme, A., et al. 2022, A&A, 659, A183
Khostovan, A. A., Sobral, D., Mobasher, B., et al. 2016, MNRAS, 463, 2363
Khusanova, Y., Le Fèvre, O., Cassata, P., et al. 2020, A&A, 634, A97
Kunth, D., & Sargent, W. L. W. 1986, ApJ, 300, 496
Kunth, D., Leitherer, C., Mas-Hesse, J. M., et al. 2003, ApJ, 597, 263
Labbé, I., Oesch, P. A., Bouwens, R. J., et al. 2013, ApJ, 777, L19
Lumbreras-Calle, A., López-Sanjuan, C., Sobral, D., et al. 2021, A&A, accepted, ArXiv e-prints [arXiv:2112.06938]
Malhotra, S., & Rhoads, J. E. 2002, ApJ, 565, L71
Martínez-Solaeche, G., González Delgado, R. M., García-Benito, R., et al. 2021, A&A, 647, A158

Martínez-Solaeche, G., González Delgado, R. M., García-Benito, R., et al. 2022, A&A, 661, A99
Maseda, M. V., van der Wel, A., Rix, H.-W., et al. 2018, ApJ, 854, 29
Matthee, J., Naidu, R. P., Pezzulli, G., et al. 2022, MNRAS, 512, 5960
Moustakas, J., & Kennicutt, R. C. 2006, ApJS, 164, 81
Naidu, R. P., Matthee, J., Oesch, P. A., et al. 2022, MNRAS, 510, 4582
Nakajima, K., Fletcher, T., Ellis, R. S., et al. 2018, MNRAS, 477, 2098
Ono, Y., Ouchi, M., Shimasaku, K., et al. 2010, ApJ, 724, 1524
Pérez-Montero, E., Vílchez, J. M., Cedrés, B., et al. 2011, A&A, 532, A141
Reddy, N. A., Shapley, A. E., Sanders, R. L., et al. 2018, ApJ, 869, 92
Salvaterra, R., Ferrara, A., & Dayal, P. 2011, MNRAS, 414, 847
Schechter, P. 1976, ApJ, 203, 297
Shirazi, M., & Brinchmann, J. 2012, MNRAS, 421, 1043
Smit, R., Bouwens, R. J., Franx, M., et al. 2015, ApJ, 801, 122
Sobral, D., & Matthee, J. 2019, A&A, 623, A157
Sobral, D., Smail, I., Best, P. N., et al. 2013, MNRAS, 428, 1128
Sobral, D., Best, P. N., Smail, I., et al. 2014, MNRAS, 437, 3516
Sobral, D., Santos, S., Matthee, J., et al. 2018a, MNRAS, 476, 4725
Sobral, D., Matthee, J., Darvish, B., et al. 2018b, MNRAS, 477, 2817
Spinoso, D., Orsi, A., López-Sanjuan, C., et al. 2020, A&A, 643, A149
Terlevich, R., Melnick, J., Masegosa, J., et al. 1991, A&AS, 91, 285
Thomas, D., Steele, O., Maraston, C., et al. 2013, MNRAS, 431, 1383
van der Wel, A., Straughn, A. N., Rix, H.-W., et al. 2011, ApJ, 742, 111
Verhamme, A., Orlitová, I., Schaerer, D., et al. 2017, A&A, 597, A13
Yang, H., Malhotra, S., Rhoads, J. E., et al. 2017, ApJ, 847, 38

[1] Instituto de Astrofísica de Andalucía – CSIC, Glorieta de la Astronomía s/n, 18008 Granada, Spain
e-mail: jiglesia@iaa.es
[2] Centro de Estudios de Física del Cosmos de Aragón, Plaza San Juan, 44001 Teruel, Spain
[3] Instituto de Física, Universidade de São Paulo, Rua do Matão 1371, CEP, 05508-090 São Paulo, Brazil
[4] Observatori Astronòmic, Universitat de València, C/ Catedrático José Beltran, 2, 46980 Paterna, València, Spain
[5] Departament d'Astronomia i Astrofísica, Universitat de València, 46100 Burjassot, València, Spain
[6] Observatório Nacional – MCTI (ON), Rua Gal. José Cristino 77, São Cristóvão 20921-400, Rio de Janeiro, Brazil
[7] Donostia International Physics Centre (DIPC), Paseo Manuel de Lardizabal 4, 20018 Donostia-San Sebastián, Spain
[8] IKERBASQUE, Basque Foundation for Science, 48013 Bilbao, Spain
[9] Instituto de Astronomia, Geofísica e Ciências Atmosféricas, Universidade de São Paulo, 05508-090 São Paulo, Brazil
[10] Instruments4, 4121 Pembury Place, La Canada Flintridge, CA 91011, USA
[11] Department of Physics, Lancaster University, Lancaster LA1 4YB, UK
[12] Departamento de Física, Faculdade de Ciências, Universidade de Lisboa, Edifício C8, Campo Grande, 1749-016 Lisbon, Portugal
[13] Departamento de Astronomia, Instituto de Física, Universidade Federal do Rio Grande do Sul (UFRGS), Av. Bento Gonçalves, 9500 Porto Alegre, RS, Brazil
[14] Instituto de Física Aplicada a las Ciencias y las Tecnologías, Universidad de Alicante, San Vicent del Raspeig, E03080 Alicante, Spain
[15] Centro de Estudios de Física del Cosmos de Aragón (CEFCA), Unidad Asociada al CSIC, Plaza San Juan 1, 44001 Teruel, Spain
[16] Département de Physique, de Génie Physique et d'Optique, Université Laval, and Centre de Recherche en Astrophysique du Québec (CRAQ), Québec, QC G1V 0A6, Canada
[17] Astronomy and Astrophysics Research and Development Department, Entoto Observatory and Research Center (EORC), Ethiopian Space Science and Technology Institute (ESSTI), PO Box 33679, Addis Ababa, Ethiopia

Appendix A: J-spectra and images of the selected EELG candidates

In this appendix we show the J-spectra and the images of the selected EELG candidates. The emission features are clearly seen in the J-spectra either for the QSOs or for the star-forming galaxies. The effect of the overlap between contiguous filters is clearly illustrated in the sources detected in more than one filter. The images show the compactness of these objects, although some low surface brightness structure is still seen for some of them.

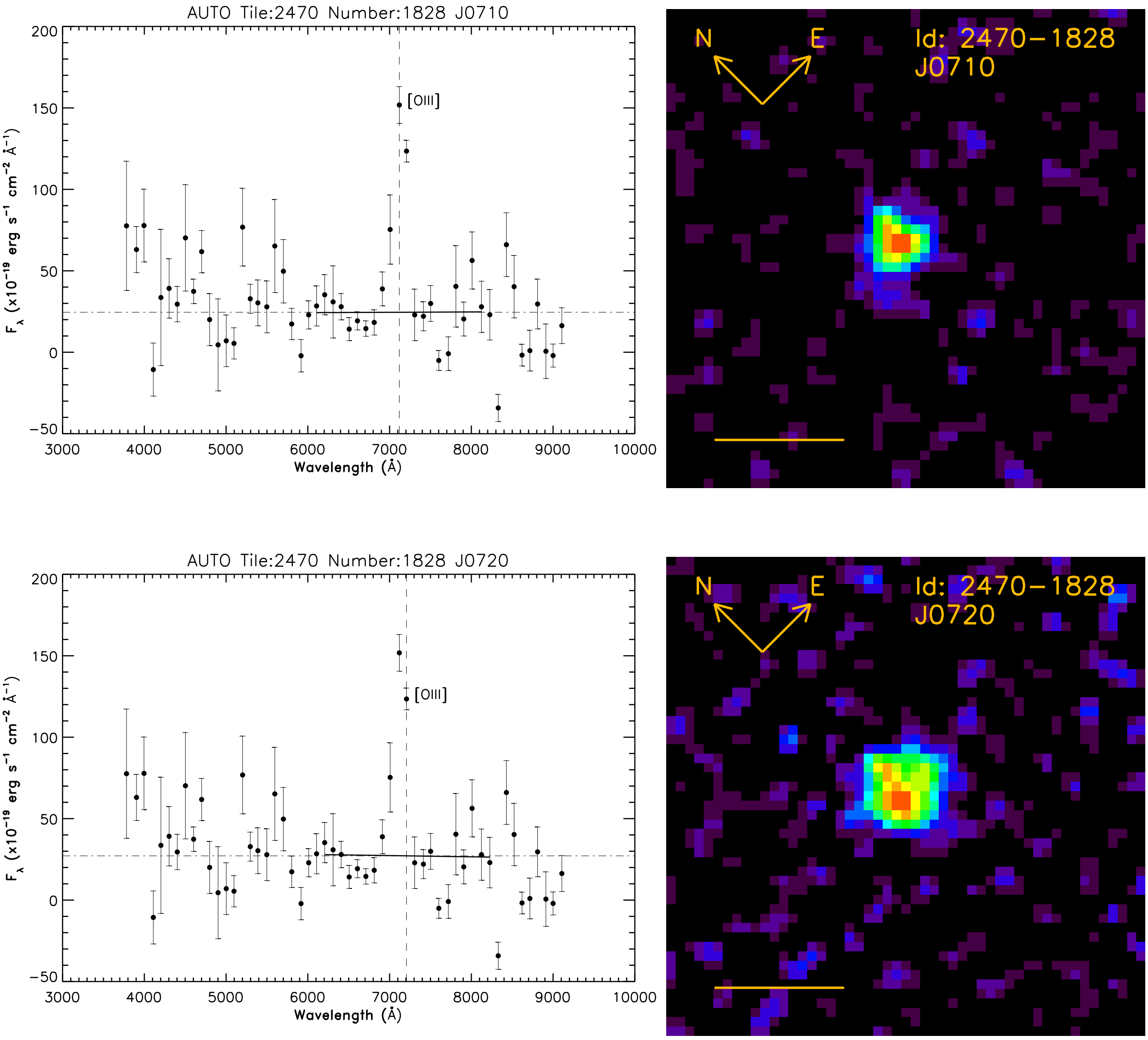

Fig. A.1. Data products from miniJPAS for the EELG candidates. Left: J-spectra using the AUTO fluxes. The vertical dashed line indicates the central wavelength of the selection filter. The solid line shows the fit to the continuum. The horizontal dot-dashed line corresponds to the continuum at the central wavelength of the selection filter. The emission line fulfilling our EW_0 condition is indicated to the right of the vertical line. Right: Cutouts of the image corresponding to the selection filter. The length of the horizontal orange line corresponds to 3".

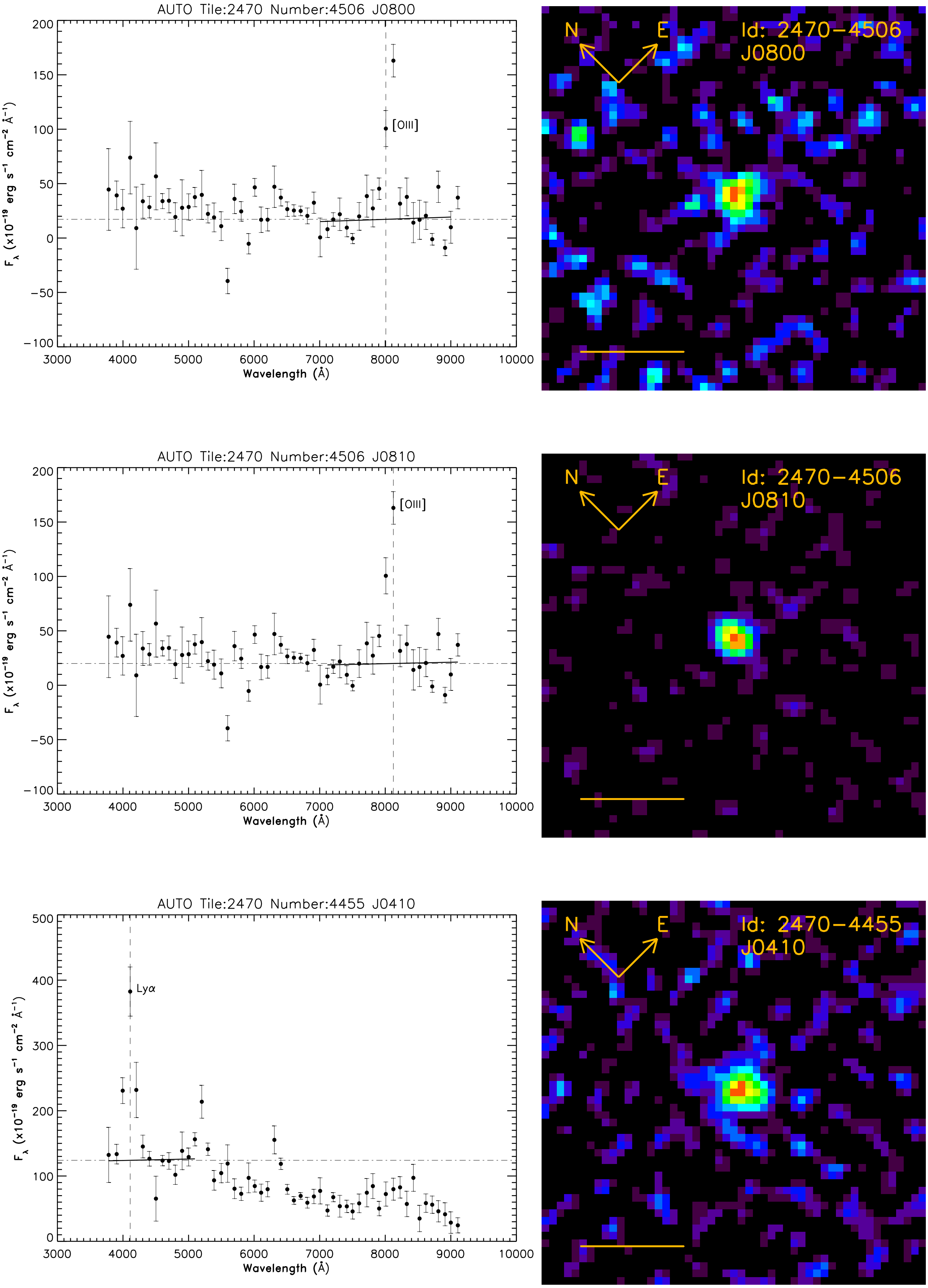

Fig. A.1. Continued.

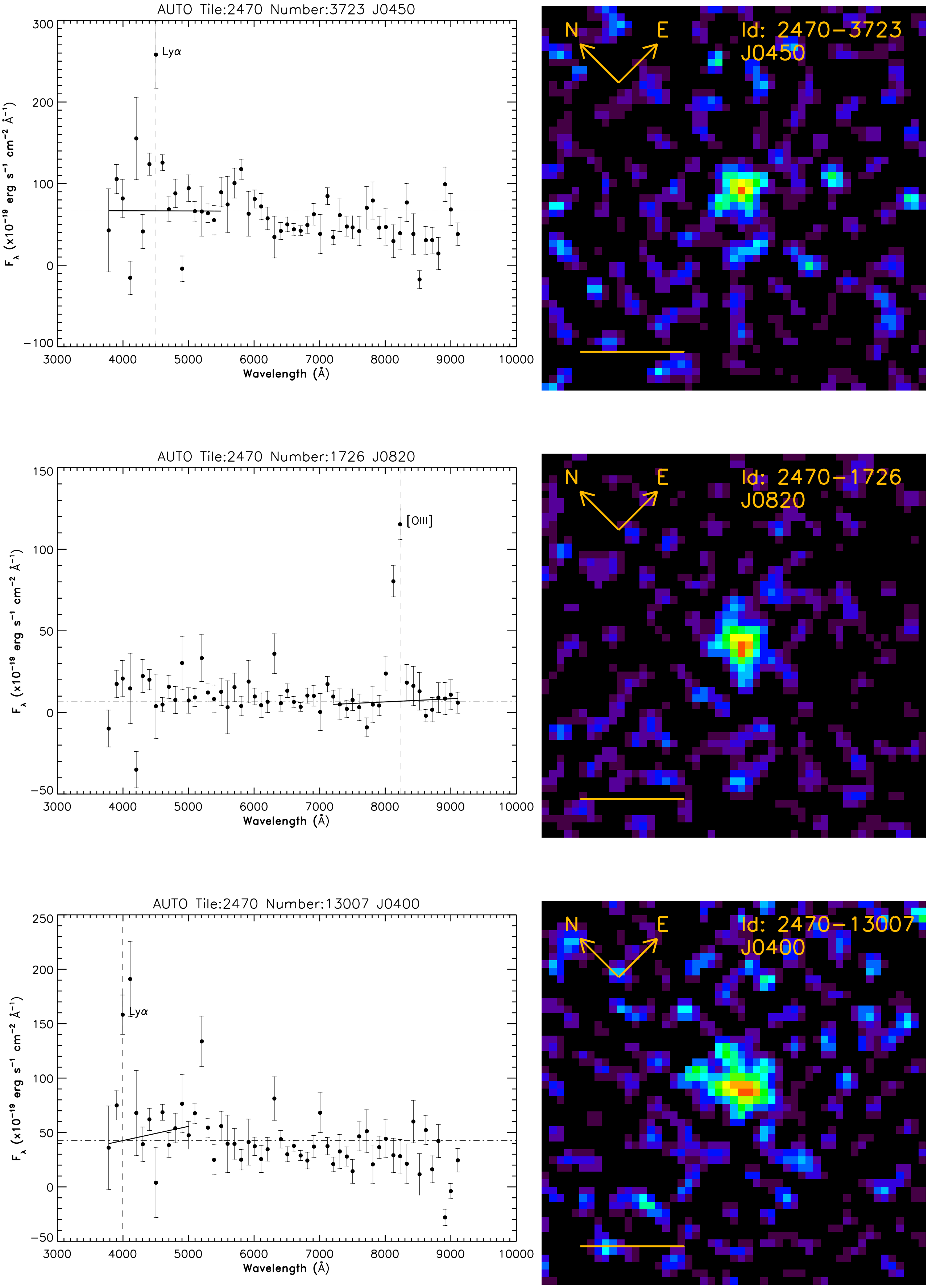

Fig. A.1. Continued.

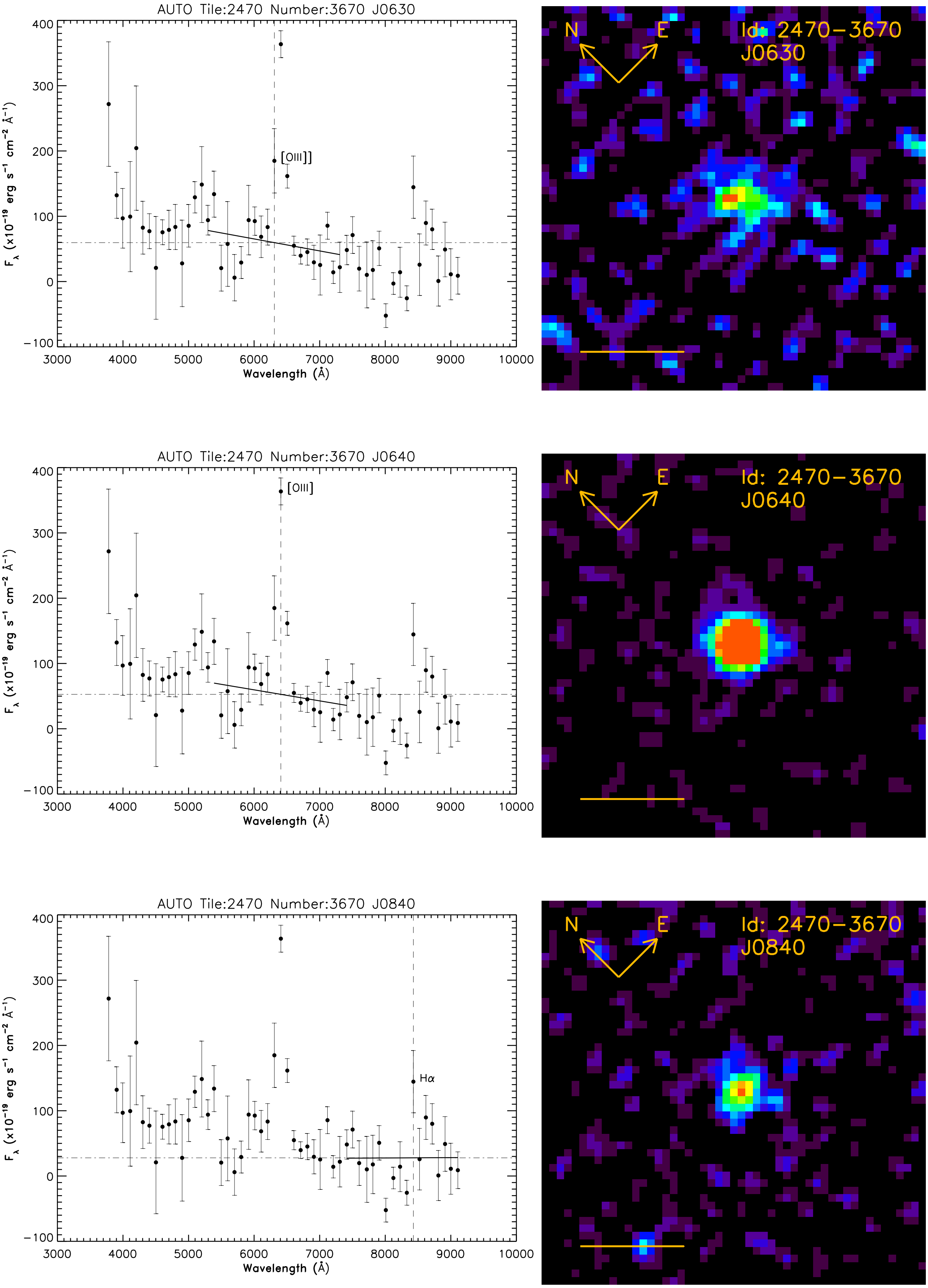

Fig. A.1. Continued.

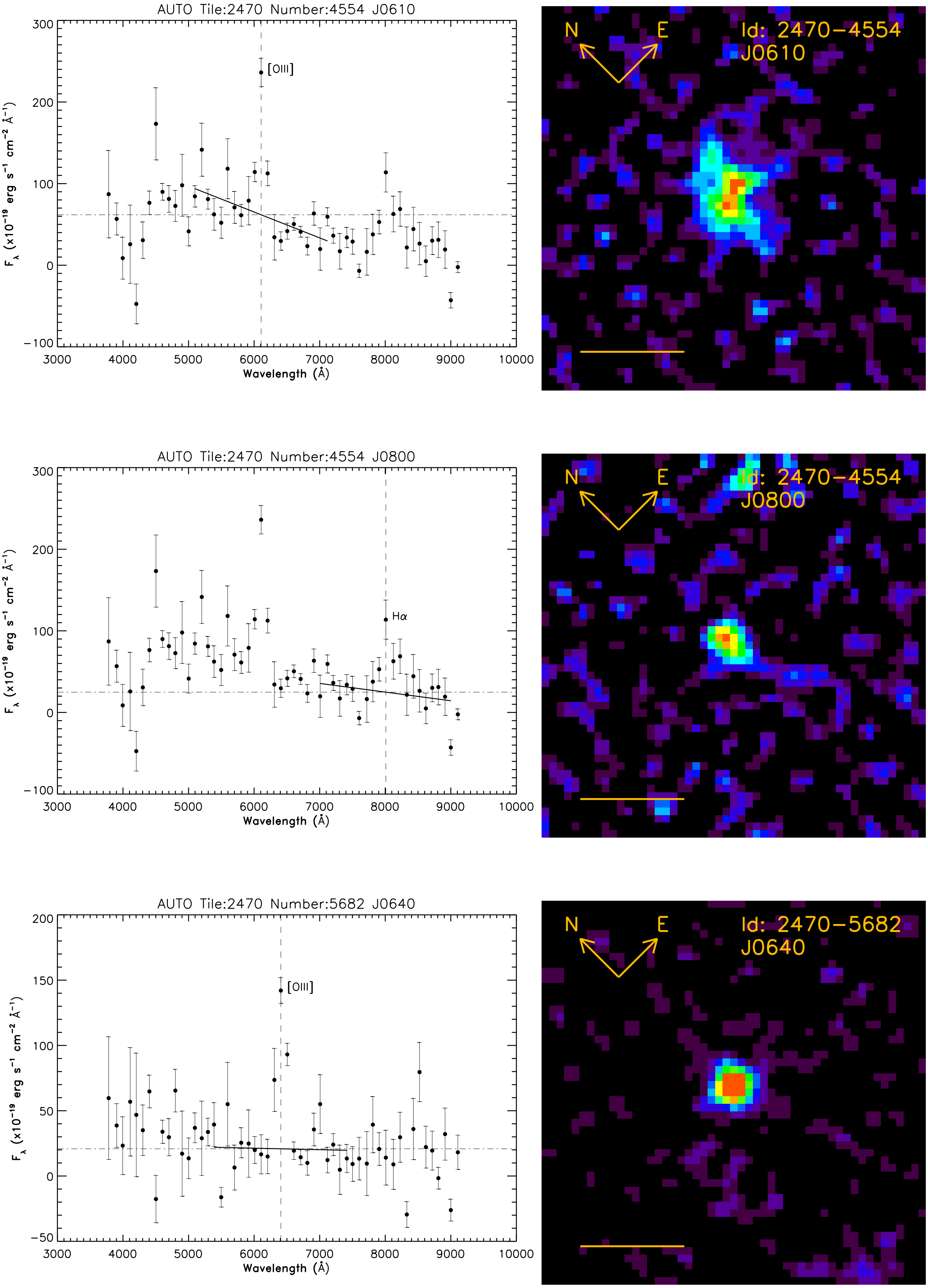

Fig. A.1. Continued.

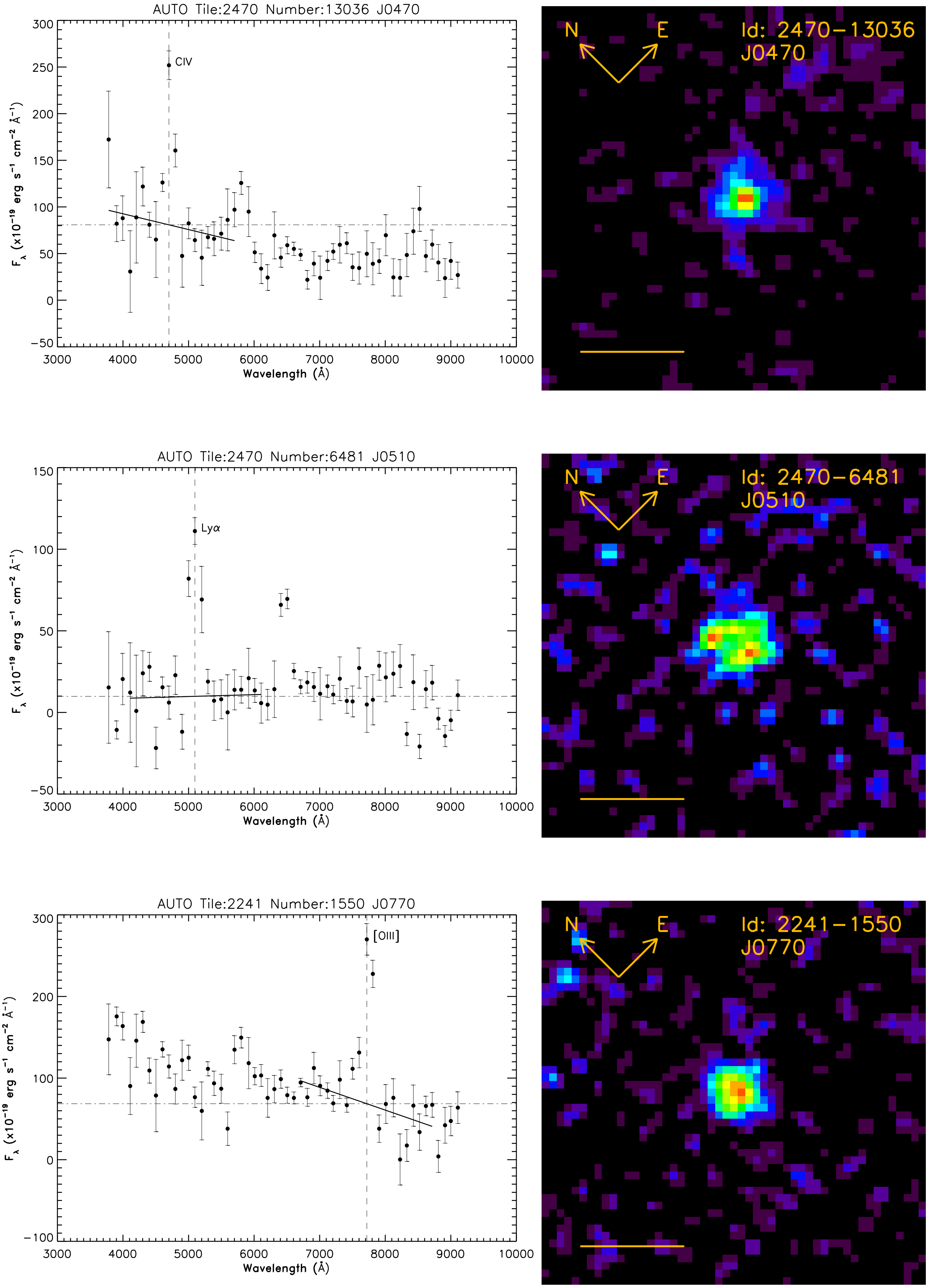

Fig. A.1. Continued.

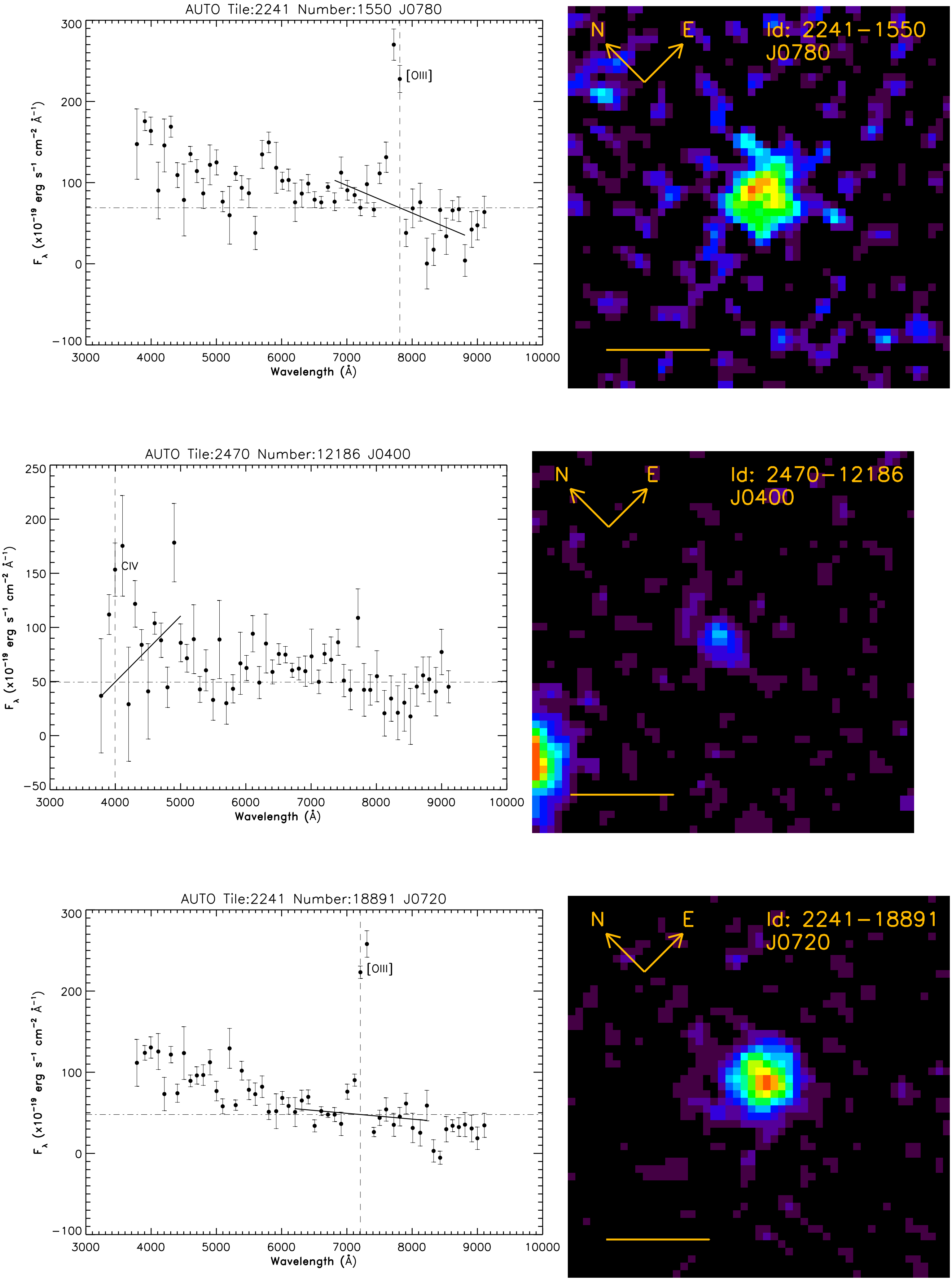

Fig. A.1. Continued.

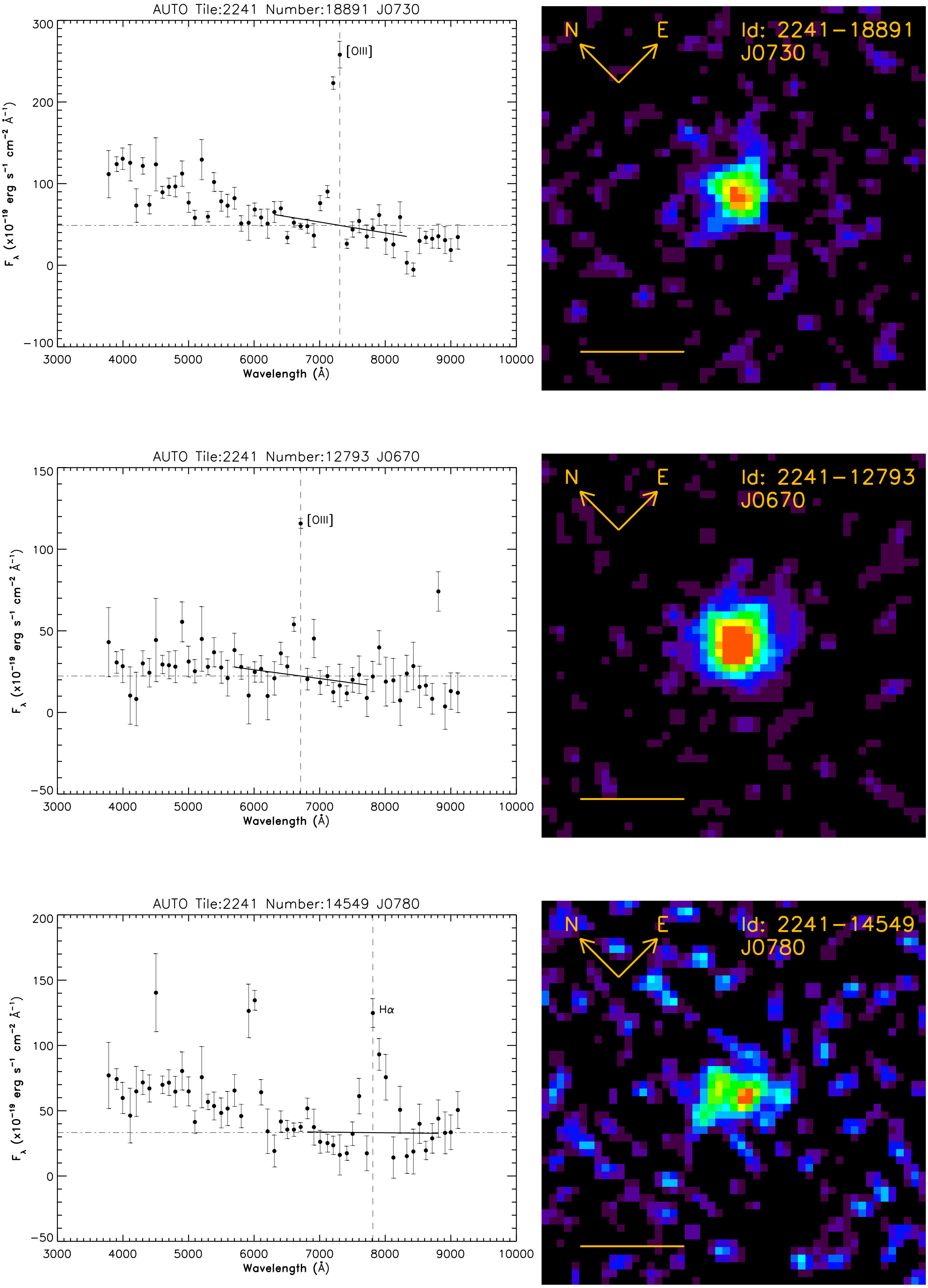

Fig. A.1. Continued.

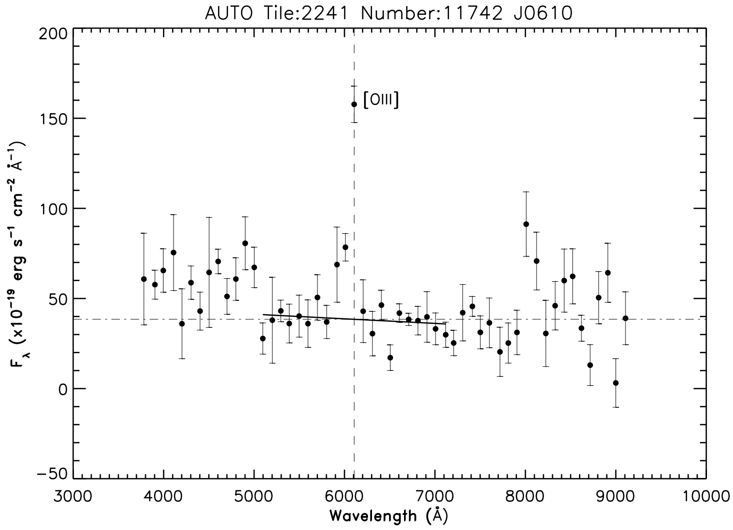

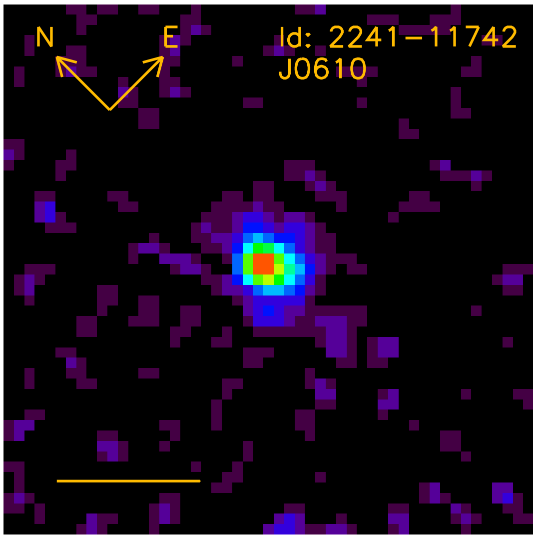

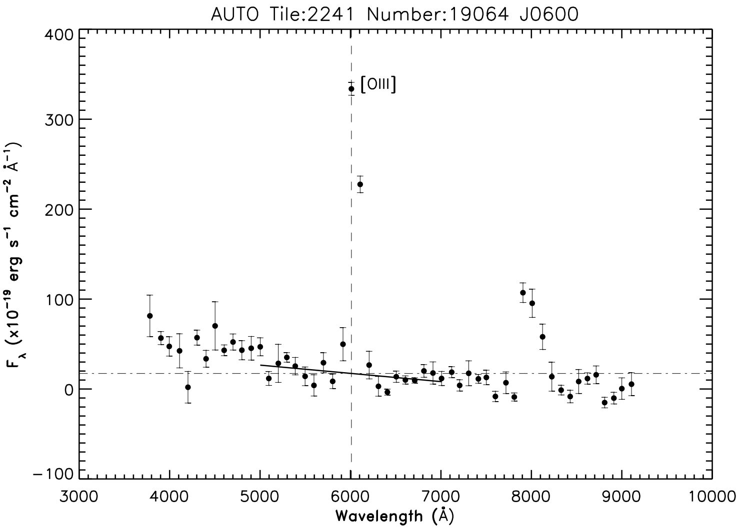

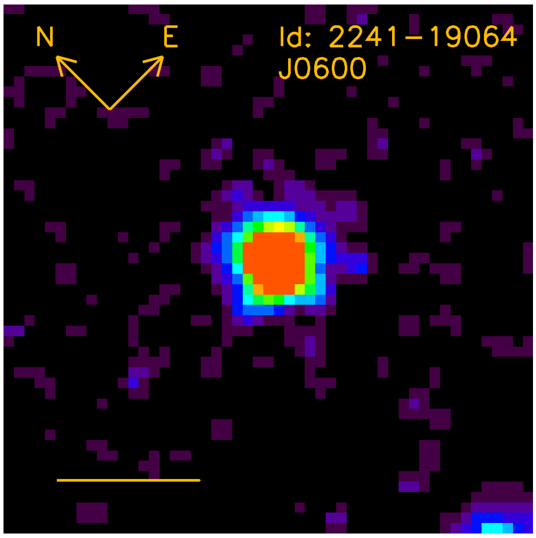

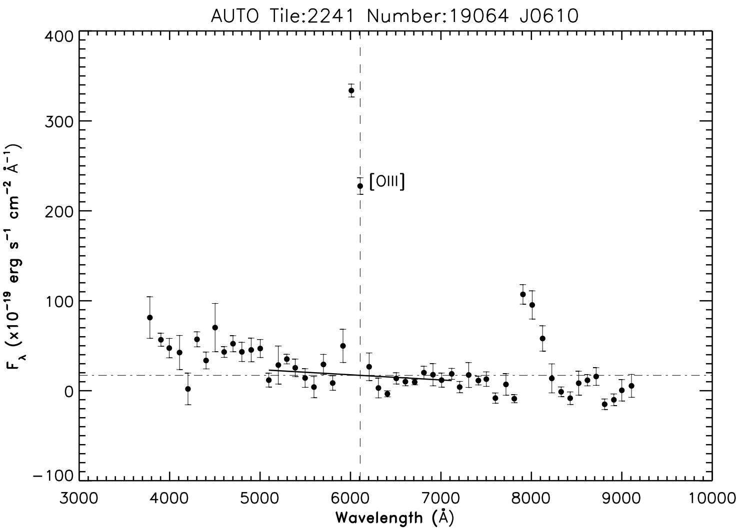

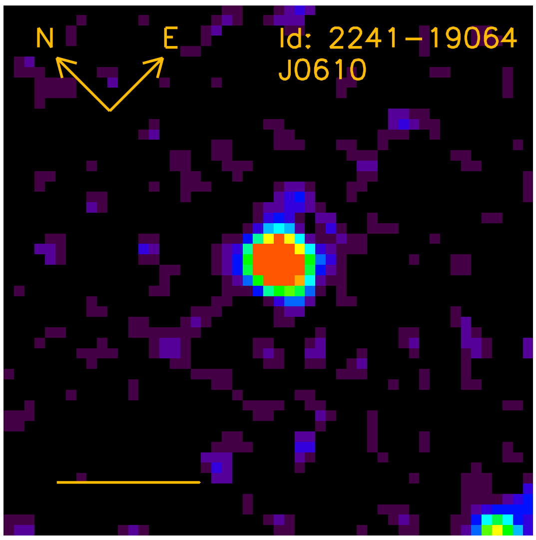

Fig. A.1. Continued.

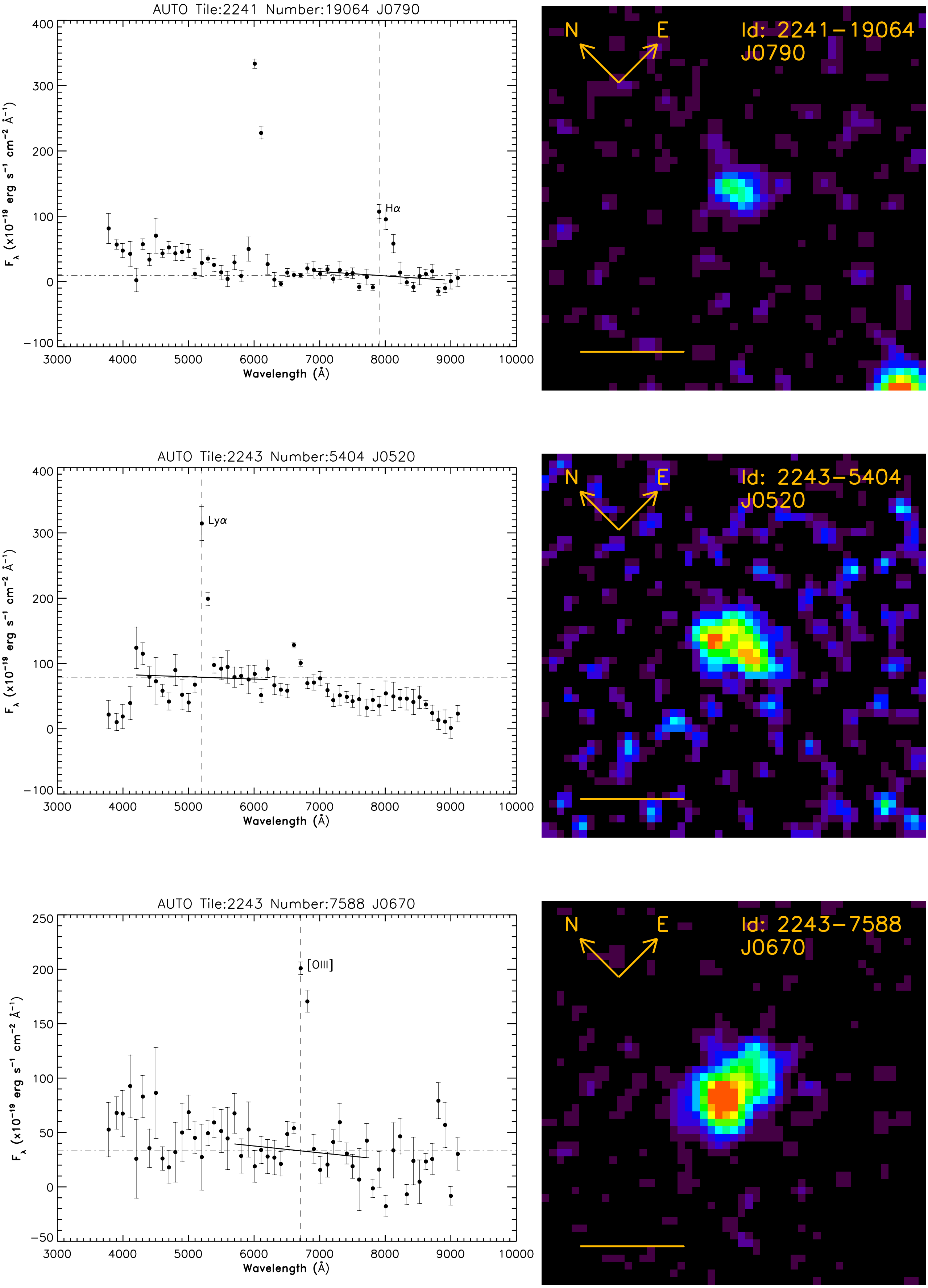

Fig. A.1. Continued.

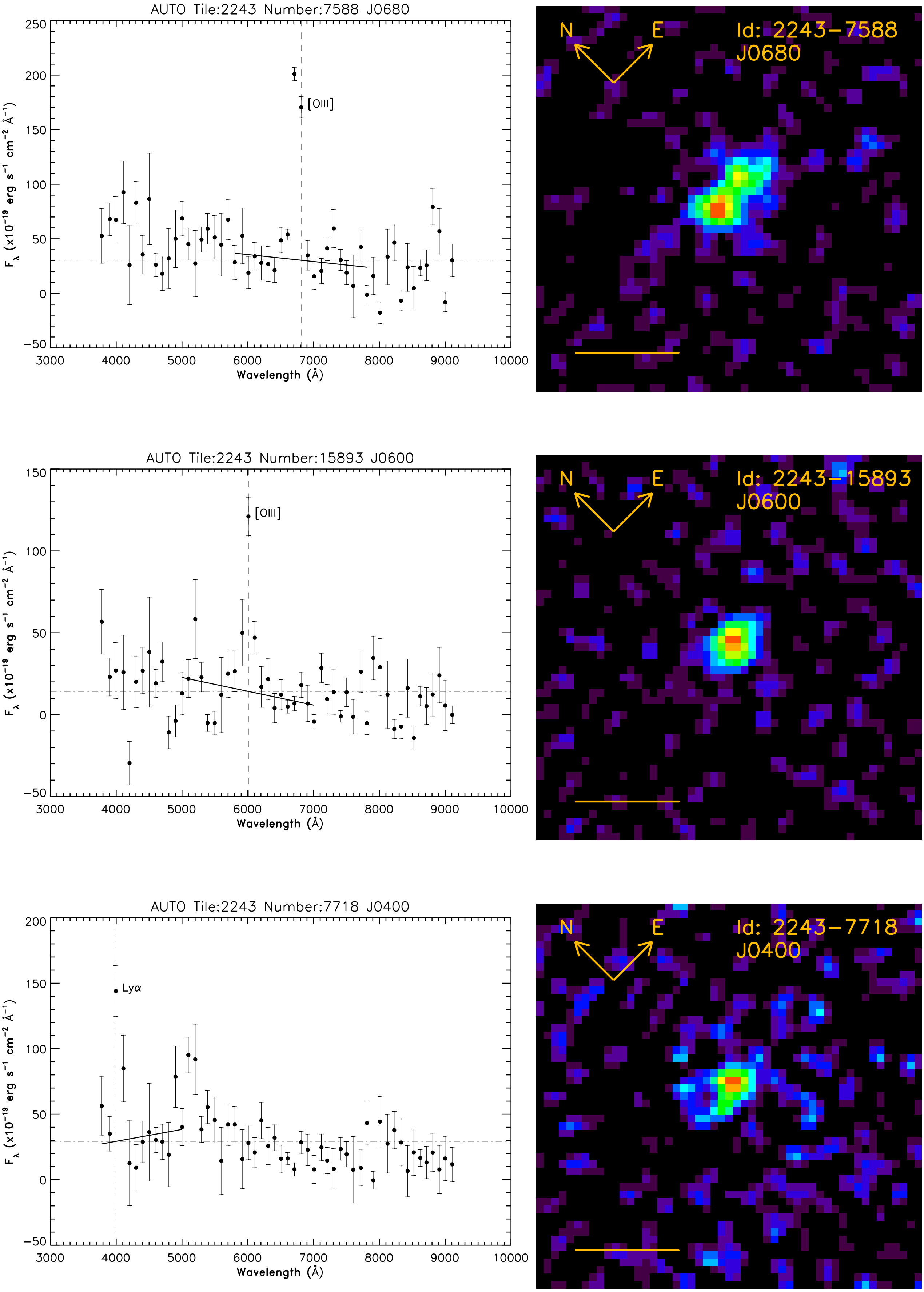

Fig. A.1. Continued.

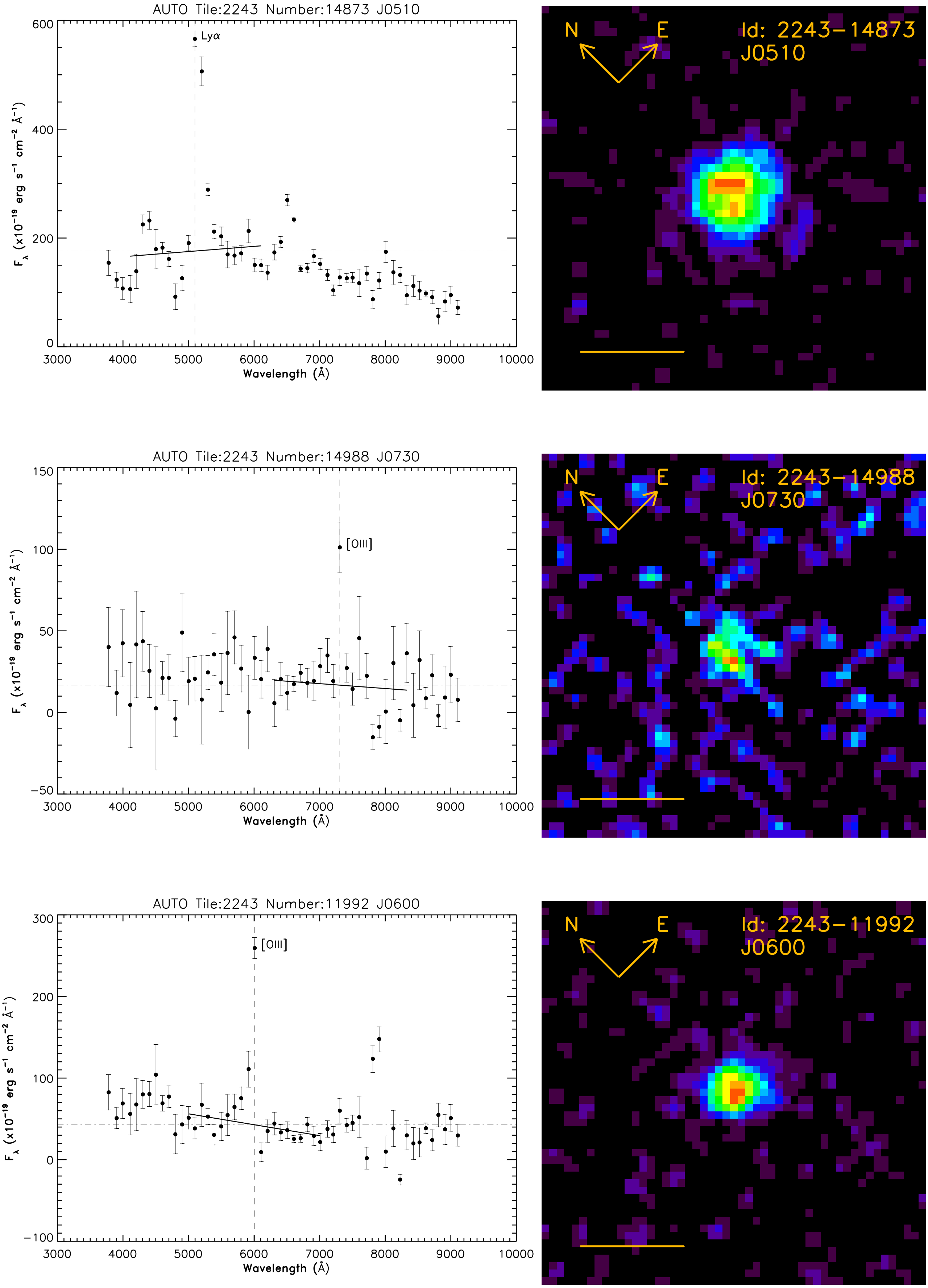

Fig. A.1. Continued.

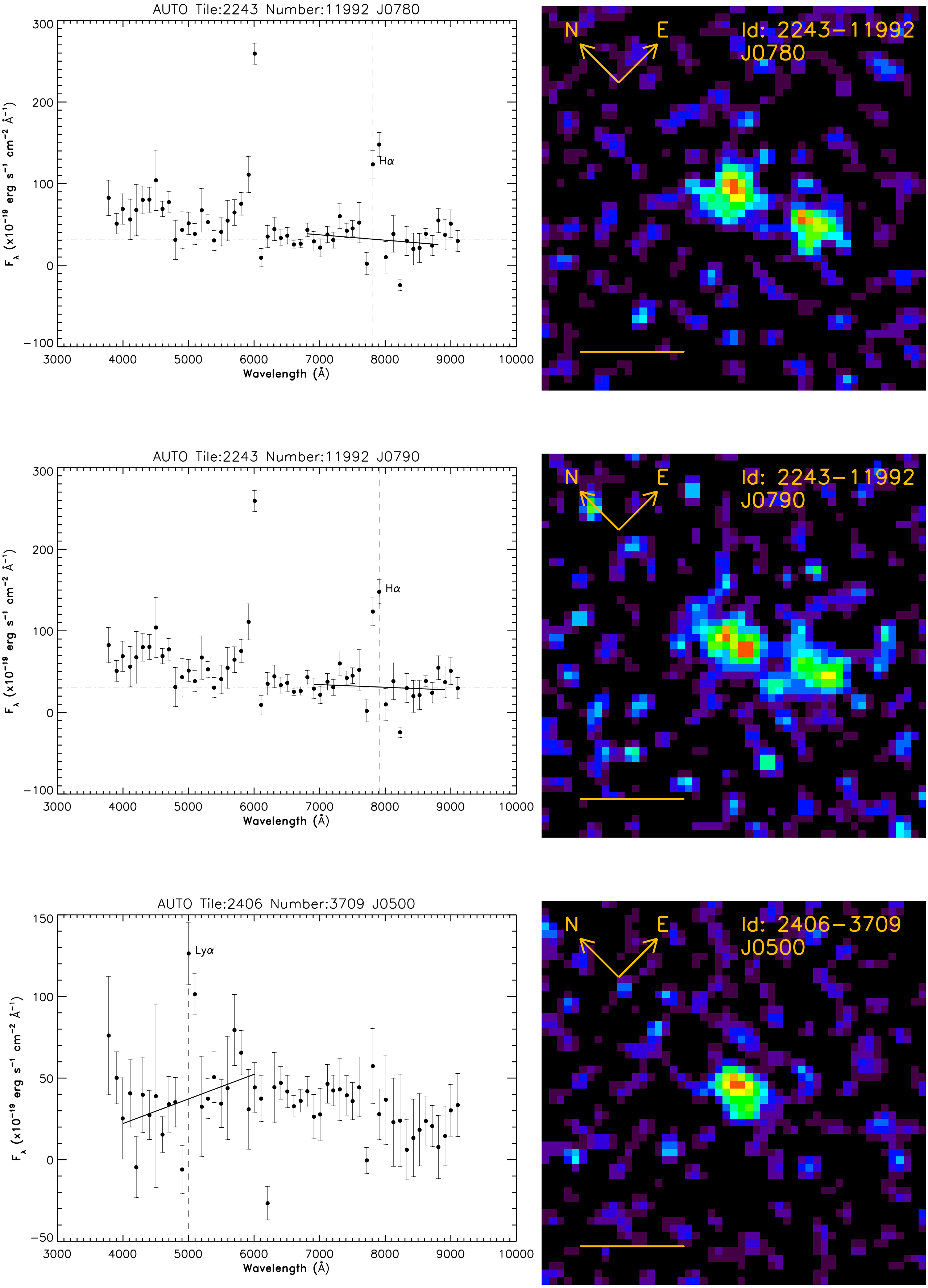

Fig. A.1. Continued.

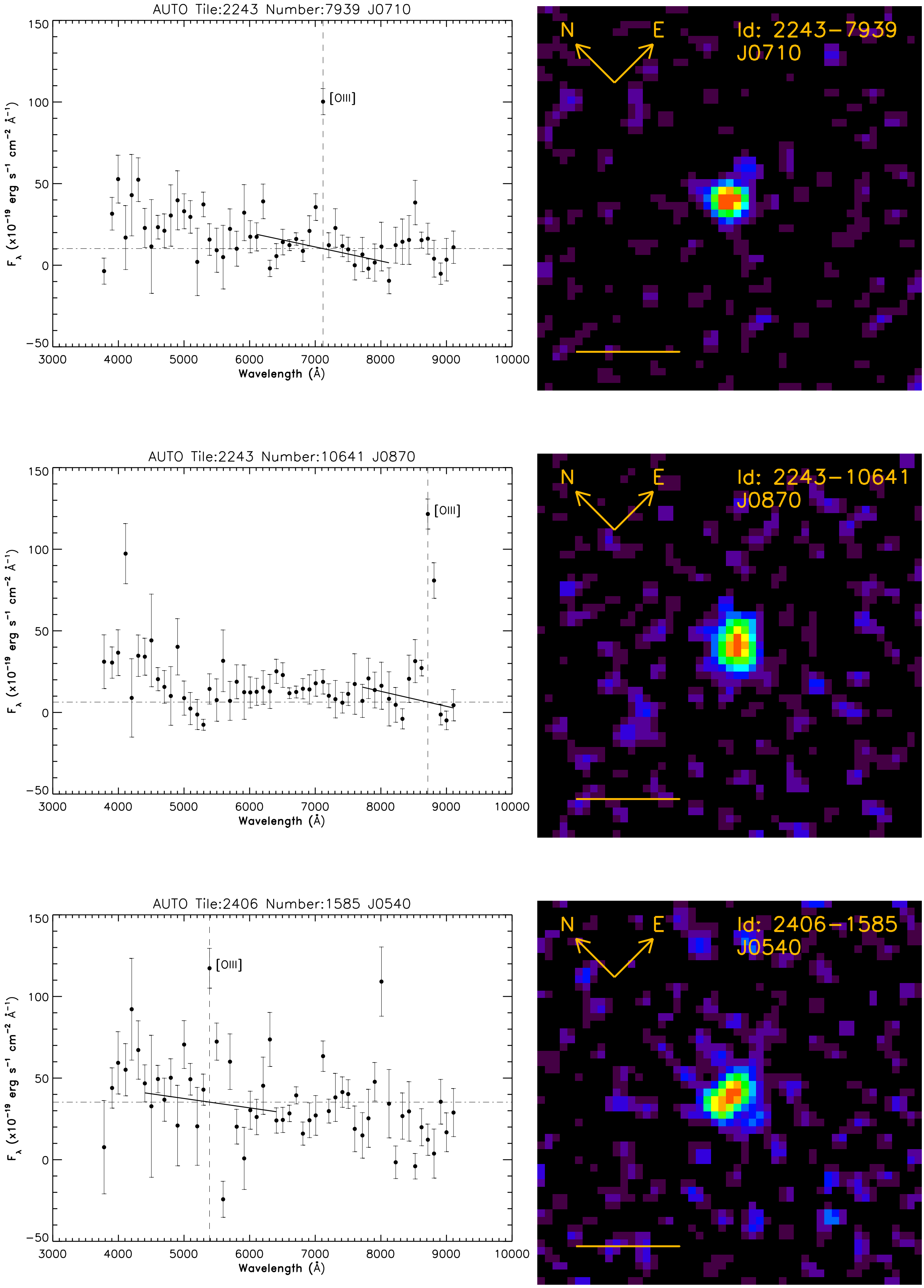

Fig. A.1. Continued.

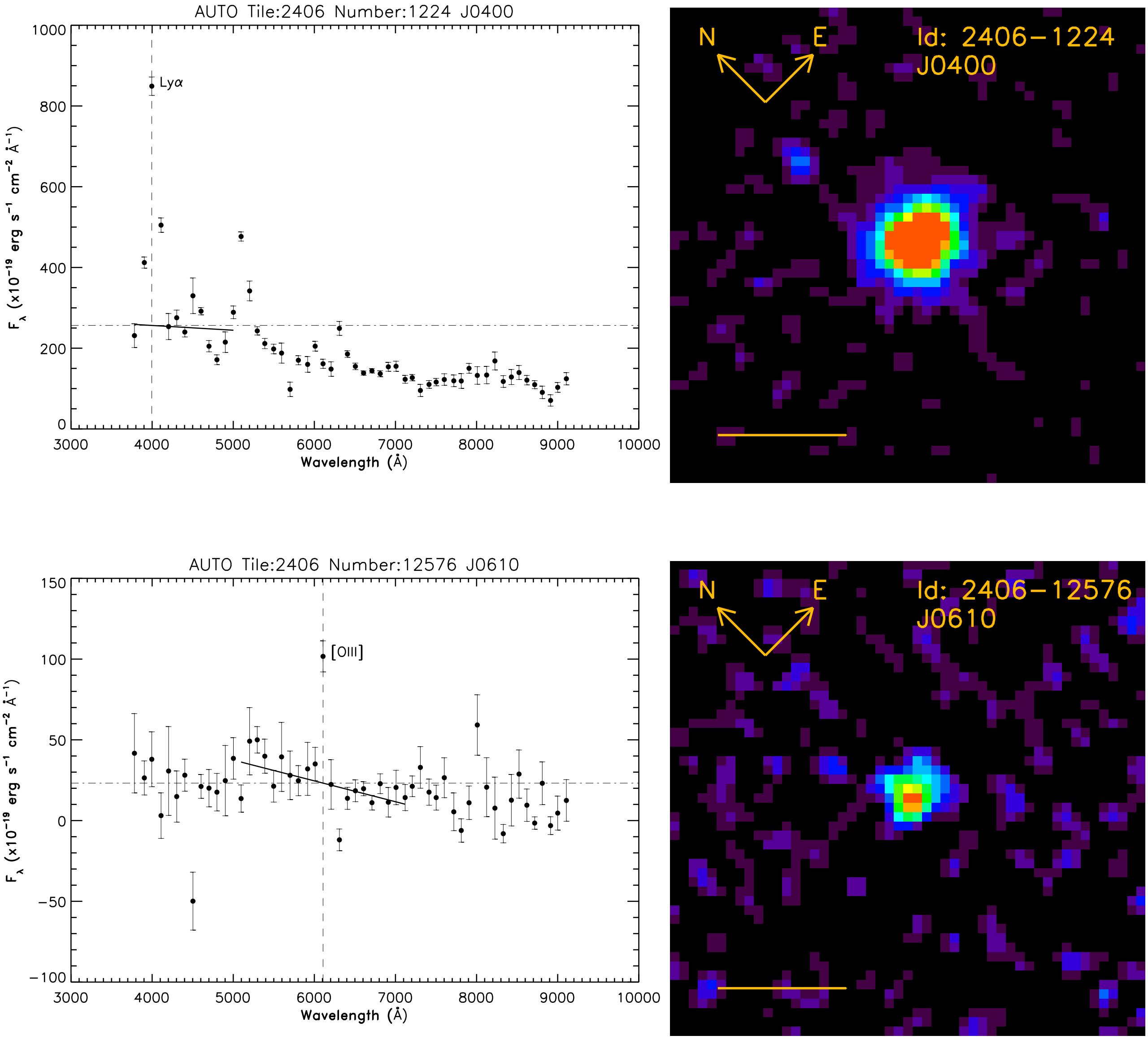

Fig. A.1. Continued.

Appendix B: Basic properties of the EELG candidates

This appendix shows the basic properties of our EELG candidates.

Table B.1. Basic properties of the EELG candidates. Uncertainties of derived quantities appear below the values in parenthesis. Objects highlighted in bold correspond to the confirmed EELGs. (1) miniJPAS identifier; (2) Right ascension (J2000.0); (3) Declination (J2000.0); (4) Stellarity index; (5) $r_{\rm SDSS}$ magnitude; (6) Filter where the object was detected; (7) Contrast; (8) Redshift estimated in this work; (9) Redshift from SDSS; (10) Redshift from DEEP2 or DEEP3; (11) Emission feature at the detection filter; (12) EW_0 of the emission feature; (13) Flux of the emission feature; (14) Luminosity of the emission feature.

Id.	R.A. (deg)	Dec. (deg)	Class	Stell. index	$r_{\rm SDSS}$ (mag)	Filter	Contrast	z (this work)	z (SDSS)	z (DEEP2/3)	Line	$EW_0^{a,b}$ (Å)	$F^{a,b}$ ($\times10^{-15}$) (erg s^{-1} cm^{-2})	log$L^{a,b}$ (erg s^{-1})
2470-1828	213.43786	52.07686	SFG	0.801	22.73	J0710	0.838	0.434	—	—	[OIII]	423	1.49	42.02
					(0.12)		(0.024)					(78)	(0.13)	(0.04)
						J0720	0.780				[OIII]	373	1.46	42.01
							(0.028)					(60)	(0.11)	(0.03)
2470-4506	213.44792	52.20433	SFG	0.073	22.44	J0800	0.829	0.614	0.613	—	[OIII]	696	1.95	42.50
					(0.08)		(0.045)					(218)	(0.39)	(0.08)
						J0810	0.877				[OIII]	613	1.97	42.50
							(0.021)					(121)	(0.20)	(0.04)
2470-4455	213.44946	52.20138	QSO	1.000	21.32	J0410	0.676	2.354	2.351	—	Lyα	92	3.86	44.24
					(0.03)		0.050					(22)	(0.62)	(0.06)
2470-3723	213.61742	52.06311	QSO	1.000	21.70	J0450	0.742	2.714	2.689	—	Lyα	114	2.82	44.25
					(0.06)		(0.053)					(30)	(0.60)	(0.09)
2470-1726	213.62304	51.95802	SFG	0.124	23.60	J0820	0.940	0.635	—	—	[OIII]	1365	1.52	42.43
					(0.15)		(0.020)					(553)	(0.14)	(0.04)
2470-13007	213.74719	52.40694	QSO	1.000	22.05	J0400	0.731	2.334	—	—	Lyα	114	1.66	43.86
					(0.06)		(0.130)					(77)	(0.35)	(0.09)
2470-3670	213.76386	51.97030	SFG	0.000	20.82	J0630	0.678	0.284	—	—	—	—	—	—
					(0.06)		(0.107)					—	—	—
						J0640	0.855				[OIII]	513	3.45	41.95
							(0.023)					(99)	(0.24)	(0.03)
						J0840	0.807				Hα	482	1.72	41.65
							(0.099)					(319)	(0.71)	(0.16)
2470-4554	213.88271	51.94262	SFG	0.000	21.53	J0610	0.738	0.226	—	—	[OIII]	267	1.99	41.49
					(0.06)		(0.028)					(39)	(0.21)	(0.04)
						J0800	0.781				Hα	422	1.27	41.29
							(0.068)					(159)	(0.35)	(0.11)
2470-5682	213.90483	51.98243	SFG	0.989	22.26	J0640	0.853	0.292	—	—	[OIII]	501	1.35	41.57
					(0.09)		(0.029)					(117)	(0.12)	(0.03)
2470-13036	213.92495	52.32272	QSO	1.000	21.46	J0470	0.679	2.044	2.036	—	CIV	102	2.52	43.90
					(0.05)		(0.036)					(17)	(0.25)	(0.04)
2470-6481	213.92791	52.15755	QSO	0.974	22.53	J0510	0.911	3.180	—	—	Lyα	368	1.52	44.15
					(0.08)		(0.033)					(168)	(0.14)	(0.04)
2241-1550	214.09392	52.30670	SFG	0.000	20.98	J0770	0.746	0.552	—	0.546	[OIII]	206	2.15	42.43
					(0.03)		(0.023)					(25)	(0.21)	(0.04)
						J0780	0.697				[OIII]	203	2.22	42.44
							(0.030)					(29)	(0.25)	(0.04)
2470-12186	214.13713	52.20877	QSO	1.000	21.58	J0400	0.678	1.624	1.600	—	CIV	98	1.38	43.39
					(0.06)		(0.190)					(86)	(0.47)	(0.14)
2241-18891	214.32208	52.53820	SFG	0.000	21.58	J0720	0.785	0.454	0.452	0.451	[OIII]	320	2.20	42.23
					(0.04)		(0.015)					(29)	(0.10)	(0.02)
						J0730	0.811				[OIII]	439	3.14	42.39
							(0.018)					(49)	(0.26)	(0.03)
2241-12793	214.34146	52.75227	SFG	0.963	22.01	J0670	0.807	0.340	—	—	[OIII]	363	1.09	41.63
					(0.04)		(0.021)					(51)	(0.04)	(0.02)
2241-14549	214.34443	52.67455	SFG	0.961	21.70	J0780	0.734	0.196	0.193	0.193	Hα	332	1.32	41.17
					(0.04)		(0.034)					(58)	(0.16)	(0.05)
2241-11742	214.38197	52.76887	SFG	0.000	21.60	J0610	0.756	0.224	—	—	[OIII]	286	1.35	41.31
					(0.04)		(0.025)					(39)	(0.12)	(0.04)
2241-19064	214.43097	52.46827	SFG	1.000	21.92	J0600	0.948	0.212	0.208	0.208	[OIII]	1758	3.58	41.68
					(0.04)		(0.007)					(259)	(0.08)	(0.01)
						J0610	0.925				[OIII]	1526	3.20	41.63
							(0.011)					(238)	(0.14)	(0.02)
						J0790	0.914				Hα	1287	1.40	41.27
							(0.023)					(416)	(0.16)	(0.04)
2243-5404	214.55589	52.87777	QSO	1.000	21.36	J0520	0.749	3.302	3.288	—	Lyα	107	3.63	44.57
					(0.04)		(0.024)					(13)	(0.40)	(0.04)

[a] The values of the EW_0(Hα), flux and luminosity have been derived assuming a line ratio [NII]λ6583Å/Hα = 0.05. [b] [OIII] corresponds to the emission line [OIII]λ5007Å.

Table B.1. Continued.

Id.	R.A. (deg)	Dec. (deg)	Class	Stell. index	$r_{\rm SDSS}$ (mag)	Filter	Contrast	z (this work)	z (SDSS)	z (DEEP2/3)	Line	$EW_0^{a,b}$ (Å)	$F^{a,b}$ ($\times10^{-15}$) (erg s^{-1} cm^{-2})	$\log L^{a,b}$ (erg s^{-1})
2243-7588	214.68784	52.94963	SFG	0.000	21.66	J0670	0.835	0.348	—	—	[OIII]	422	1.87	41.89
					(0.06)		(0.019)					(60)	(0.08)	(0.02)
						J0680	0.822				[OIII]	502	2.08	41.94
							(0.024)					(84)	(0.16)	(0.03)
2243-15893	214.69939	53.03229	SFG	0.472	22.73	J0600	0.883	0.206	—	—	[OIII]	718	1.21	41.18
					(0.12)		(0.026)					(181)	(0.14)	(0.05)
2243-7718	214.87076	52.83314	QSO	0.414	22.60	J0400	0.797	2.322	—	—	Lyα	176	1.74	43.87
					(0.12)		(0.099)					(109)	(0.35)	(0.08)
2243-14873	214.89826	52.95298	QSO	1.000	20.42	J0510	0.689	3.226	3.218	—	Lyα	77	5.77	44.74
					(0.02)		(0.012)					(4)	(0.24)	(0.02)
2243-14988	214.91904	52.94645	SFG	0.846	22.63	J0730	0.835	0.464	—	0.461	[OIII]	383	0.94	41.88
					(0.13)		(0.042)					(119)	(0.18)	(0.08)
2243-11992	214.92816	53.07305	SFG	0.000	21.69	J0600	0.835	0.200	—	0.198	[OIII]	477	2.45	41.46
					(0.05)		(0.015)					(53)	(0.16)	(0.03)
						J0780	0.742				Hα	419	1.59	41.27
							(0.044)					(95)	(0.29)	(0.07)
						J0790	0.789				Hα	444	1.67	41.29
							(0.030)					(83)	(0.22)	(0.05)
2406-3709	214.98989	53.20826	QSO	0.001	21.96	J0500	0.705	3.162	—	—	Lyα	85	1.35	44.09
					(0.08)		(0.064)					(26)	(0.30)	(0.09)
2243-7939	215.00404	52.74137	SFG	0.002	22.96	J0710	0.898	0.424	—	—	[OIII]	686	0.99	41.81
					(0.12)		(0.022)					(182)	(0.09)	(0.03)
2243-10641	215.24110	52.94494	SFG	0.263	23.25	J0870	0.948	0.748	—	0.747	[OIII]	1236	1.29	42.53
					(0.15)		(0.029)					(902)	(0.11)	(0.03)
2406-1585	215.31301	52.92023	SFG	0.000	22.14	J0540	0.699	0.086	—	—	[OIII]	245	0.93	40.24
					(0.07)		(0.048)					(55)	(0.14)	(0.06)
2406-1224	215.32499	52.89611	QSO	1.000	20.53	J0400	0.698	2.304	2.305	—	Lyα	101	8.57	44.56
					(0.02)		(0.021)					(9)	(0.39)	(0.02)
2406-12576	215.77825	53.18870	SFG	0.972	22.73	J0610	0.772	0.218	—	—	[OIII]	392	1.11	41.20
					(0.10)		(0.033)					(74)	(0.14)	(0.05)